Title: Molecular Disambiguation of Heart Rate Control by the Nucleus Ambiguus

Running Title: Classifying Ambiguus Cardiovagal Neurons

Authors: Jalil, Maira[1] <mj5an@virginia.edu>; MacMillan, Mary Katherine[2] <qzc7nn@virginia.edu>; Gutierrez, Veronica A.[1] <vag2pg@virginia.edu>; Crook, Maisie E.[1] <mc5wp@virginia.edu>; Coverdell, Tatiana C.[3] <tatiana.coverdell@gmail.com>; Dever, Ashlyn[1] <pqz9vu@virginia.edu>; Cox, Katie Shouse[1] <ks3ve@virginia.edu>; Stornetta, Daniel S.[3] <dss2q@virginia.edu>; Wang, Yoko B.[4] <yokowang@missouri.edu>; Schwalbe, Dana C.[1] <dana_schwalbe@g.harvard.edu>; Singh, Adriana[1] <acu4ej@virginia.edu>; VanderVoort, Lane[1] <uaa3sk@virginia.edu>; Boychuk, Carie R.[4] <boychukc@missouri.edu>, Abbott, Stephen B. G.[† 2,3] <sba6t@virginia.edu>; Campbell, John N. [† 1,2] <jnc4e@virginia.edu>

[†] *equally contributing senior author*

[1] Department of Biology, University of Virginia, Charlottesville, VA

[2] Neuroscience Graduate Program, University of Virginia, Charlottesville, VA

[3] Department of Pharmacology, University of Virginia, Charlottesville, VA

[4] Dalton Cardiovascular Research Center, University of Missouri, Columbia, MO, USA

Correspondence to:

John N. Campbell (lead contact), Department of Biology, University of Virginia, 485 McCormick Road, PO BOX 4000328, Charlottesville, VA 22904; e-mail: jnc4e@virginia.edu

and

Stephen B. G. Abbott, Department of Pharmacology, University of Virginia, 1340 Jefferson Park Avenue, Charlottesville, VA 22908; e-mail: sba6t@virginia.edu

Key words: Nucleus ambiguus; Cardiovagal neurons; Heart rate regulation; Parasympathetic nervous system; Vagus nerve; Single-cell RNA-sequencing; Diving reflex

Acknowledgements: We gratefully acknowledge Patrice G. Guyenet, Ruth Stornetta, and Steven J. Swoap for thoughtful discussion and feedback on the experimental design; Bradford B. Lowell for the Chat-Flp mouse line; Stephen D. Liberles for the Npy2r-Cre mouse line; Patrice G. Guyenet and Hui Zong for co-acquisition of pilot funding; and Moon Snyder, Natalie Schiavone, and Virginia Owen Trinkle for technical support. We also acknowledge the valuable assistance of these UVA core facilities: the Robert M. Berne Cardiovascular Research Center Histology Core; the Biology Department Genomics Core; the Genome Analysis and Technology Core (RRID:SCR_018883); and the Flow Cytometry Core Facility.

Funding statement: Funding was provided by a University of Virginia 3 Cavaliers award to J.N.C., Patrice G. Guyenet, and Hui Zong; NIH R01 HL148004 to SBGA; NIH T32 GM007055 and NIH F31 HL158187 to TCC; and a Pathway to Stop Diabetes Initiator Award 1-18-INI-14 and NIH R01 HL153916 to JNC.

Data availability statement: The raw and processed single-nuclei RNA-seq data and metadata reported in this paper are available at GEO accession number ######. A user-friendly interface for visualizing and exploring the single-nuclei RNA-seq data is available at the Broad Institute Single Cell Portal at ######. The code used for processing, clustering, and visualizing the clustered single-nuclei RNA-seq data is available through Zenodo at ######. Any additional information required to reanalyze the data reported in this paper is available from the lead contact upon reasonable request.

Conflict of interest disclosure: The authors declare no conflict of interest

Ethics approval statement: All animal care and experimental procedures were approved in advance by the University of Virginia Institutional Animal Care and Use Committee under animal use protocols #4232 and #4354.

Patient consent statement: not applicable

Permission to reproduce material from other sources: not applicable

Clinical trial registration: not applicable

ABSTRACT

The nucleus ambiguus (nAmb) provides parasympathetic control of cardiorespiratory functions as well as motor control of the upper airways and esophagus. A subset of nAmb neurons innervates the heart through the vagus nerve to control cardiac function at rest and during key autonomic reflexes such as the mammalian diving reflex. Yet, how these cardiovagal nAmb neurons differ from other nAmb neurons in the adult brain remains unclear. We therefore classified adult mouse nAmb neurons molecularly, anatomically, and functionally. First, our integrated analysis of single-nucleus RNA-sequencing data predicted multiple molecular subtypes of nAmb neurons. Mapping the axon projections of one nAmb neuron subtype, *Npy2r*-expressing nAmb neurons, showed that they innervate cardiac ganglia but not the upper airways or esophagus. Chemogenetically stimulating *Npy2r*+ nAmb neurons robustly decreased heart rate through peripheral muscarinic acetylcholine receptors. Finally, *Npy2r*+ nAmb neurons are activated during voluntary underwater diving, consistent with a cardiovagal function for this

nAmb subtype. These results together reveal the molecular organization of nAmb neurons and its control of heart rate.

INTRODUCTION

The parasympathetic nervous system powerfully slows heart rate by signaling through the vagus nerve. This was famously demonstrated in the mid-19th century by the Weber brothers, who found that electrically stimulating the vagus nerve slowed, and in some cases stopped, the hearts of frogs and mammals [1,2]. Tonic cardiovagal signaling sets resting HR and mediates autonomic reflexes such as the baroreflex, respiratory sinus arrhythmia, and mammalian diving reflex [3-6]. The diving reflex, for instance, first described by Edmund Goodwyn in 1786 [7,8], is one of the most robust and evolutionarily conserved of autonomic reflexes [6,9,10]. This reflex occurs when holding breath underwater and triggers a dramatic decrease in heart rate (bradycardia), likely to conserve oxygen stores during an underwater dive [11].

Cardiovagal fibers originate primarily from two medullary regions, the nucleus ambiguus (nAmb) and the dorsal motor nucleus of the vagus (DMV) [12-14]. Cardiovagal axons project through the vagus nerve to synapse on postganglionic parasympathetic neurons in cardiac ganglia [15,16]. At these ganglionic synapses, cardiovagal release of acetylcholine (ACh) activates cardiac neurons via α4β2 nicotinic ACh receptors [17] while potentially suppressing sympathetic input to the same neurons [18]. CVNs may release other signaling molecules as well – for instance, neuropeptides such as PACAP (gene, *Adcyap1*) to modulate cardiac neuron excitability [19,20] and vasoactive intestinal peptide (VIP; gene, *Vip*) to control coronary artery flow [21,22]. In turn, cardiac neurons synapse on cardiomyocytes in the sinoatrial (SA) and atrioventricular (AV) nodes, where their release of acetylcholine (ACh) on muscarinic acetylcholine receptors slows cardiomyocyte electrical conduction and consequently decreases heart rate, AV conduction,

105 and ventricular contractility. Vagotomy or blocking muscarinic receptors increases heart rate,
106 indicating that parasympathetic tone sets heart rate at rest [23-25].
107
108 Previous studies suggest the nAmb plays a larger role than the DMV in setting heart rate at rest
109 and during reflexes such as the diving reflex [26-31]. However, the nAmb is a functionally
110 heterogeneous region which, in addition to its cardiovagal neurons, also contains respiratory
111 parasympathetic neurons and motor neurons for the upper airways and esophagus [5,32-35].
112 Recent findings have raised the possibility that the nAmb's functional roles are delegated to
113 different molecular subtypes of nAmb neurons [5,36,37]. Yet, a comprehensive understanding of
114 these molecular subtypes in the adult brain and their anatomical and functional differences is
115 still lacking. We used single-cell transcriptomics and anatomical tracing to define nAmb neuron
116 subtypes and identified one that innervates cardiac ganglia, decreases heart rate upon
117 activation, and is engaged during the diving reflex.
118
119 **RESULTS**
120
121 *Molecular Classification of Nucleus Ambiguus Neurons in the Adult Mouse*
122
123 To classify molecular subtypes of nucleus ambiguus (nAmb) neurons in adult mice, we
124 compared their genome-wide RNA expression using single-nuclei RNA sequencing (snRNA-
125 seq). First, to enrich for nAmb neurons, we fluorescently labeled their cell nuclei based on
126 expression of the cholinergic marker gene, *Chat,* which encodes choline acetyltransferase
127 (ChAT) and which all nAmb vagal efferents and few neighboring cells express [36] (Supplemental
128 Figure 1A). Specifically, we crossed mice in which Cre recombinase expression is driven by the
129 *Chat* gene (Chat-Cre) [38], to mice which Cre-dependently express a nuclear-localized mCherry
130 fluorescent protein (H2b-mCherry; "H2b-TRAP" mice). The resulting Chat-Cre::H2b-TRAP mice

131 exhibited H2b-mCherry expression in all peripherally projecting nAmb neurons [36] (Supplemental
132 Figure 1B). As a complementary approach, to avoid any cells labeled due to Chat-Cre
133 expression only during development, we injected the nAmb of other adult Chat-Cre mice with an
134 adeno-associated virus (AAV) that Cre-dependently expresses H2b-mCherry. We then isolated
135 mCherry+ cell nuclei from dissected nAmb tissue samples, processed their poly-adenylated
136 RNA into sequencing libraries, and sequenced them (Figure 1A).
137
138 Our initial dataset contained 3,490 nuclear transcriptomes ("cells") across three batches
139 (Supplemental Figure 1C). Filtering out low-quality transcriptomes and likely cell doublets left
140 3,461 cells for further analysis. Grouping the pass-filter cells by their expression of high-
141 variance genes yielded 18 clusters (annotated as c1-c18), each containing cells from each
142 sample batch (Supplemental Figure 1D-G). To identify the nAmb neuron clusters, we plotted
143 expression of positive marker genes associated with cholinergic and motor neurons
144 (vAChT/*Slc18a3*, *Isl1*, *Chat*) and negative marker genes (*Slc32a1*, *Slc17a6*) which are
145 expressed around but not in the nAmb [36,39-41] (Supplemental Figure 1H). Based on our results,
146 we annotated five clusters, containing 1,245 neurons in total, as candidate subtypes of nAmb
147 neurons (Supplemental Figure 1H).
148
149 We further explored the molecular heterogeneity of nAmb neurons by re-clustering them apart
150 from non-nAmb neurons. This resulted in six transcriptionally distinct clusters (n1-n6) in which
151 we detected on average (+/- standard deviation, S.D.) 2,927 +/- 967 genes per neuron, based
152 on 6,666 +/- 3,565 unique transcripts per neuron (Figure 1B). Each cluster contained cells from
153 each sample batch (Supplemental Figure 1I-J). Comparing the neuron clusters revealed many
154 differentially expressed genes (Figure 1C; Supplemental Figure 1K). Among these was the gene
155 *Adcyap1*, which is enriched in clusters n02 and n03 (Supplemental Figure 1K) and encodes
156 pituitary adenylate cyclase activating polypeptide (PACAP), a neuropeptide found in cholinergic

157 axons innervating the heart in guinea pigs [19]. These results suggest that clusters n02 and n03
158 may contain cardiovagal neurons.
159
160 We then examined the expression of marker genes reported in previous studies. One of these
161 studies, Coverdell et al., 2022, identified three molecular subtypes among 141 adult mouse
162 nAmb neurons: Crhr2^{nAmb} neurons, which control esophageal motor function; Vipr2^{nAmb} neurons,
163 which innervate the pharynx and larynx; and Adcyap1^{nAmb} neurons, whose anatomy and function
164 were unknown [36]. Another study, Veerakumar et al. 2022, characterized three molecular
165 subtypes from 203 neonatal mouse nAmb neurons innervating the larynx or heart: ACP neurons
166 and ACV neurons, which can alter cardiopulmonary and cardiovascular function, respectively,
167 and larynx-projecting neurons [37]. When we plotted the expression of these published marker
168 genes in our dataset, we found that clusters n01, n02 and n03 likely correspond to cardiovagal
169 parasympathetic motor neurons, whereas clusters n04, n05 and n06 aligned to branchial motor
170 neurons that innervate skeletal muscles of the upper airway and esophagus (Figure 1D).
171
172 Cluster n03 expressed markers of two previously defined subtypes of cardiovagal neurons, ACP
173 neurons and ACV neurons (Figure 1D), suggesting heterogeneity within this cluster. Re-
174 clustering only the neurons from n03 resolved four sub-clusters (n03.s01-04; Figure 1E). One of
175 these sub-clsuters expressed a marker of ACV neurons (*Bche*), while another expressed a
176 marker of ACP neurons (*Calb1*; Figure 1F). Interestingly, the putative ACV neurons also
177 expressed *Npy2r*, the gene encoding the neuropeptide Y2 receptor, which modulates vagal
178 control of heart rate [42] and is also expressed by vagal sensory neurons that control heart rate [42-
179 44]. Together, our results identify five candidate molecular subtypes of neurons in the adult nAmb
180 and raise the possibility that *Npy2r*$^{+}$ nAmb neurons contribute to heart-rate control.
181

182 To compare our nAmb neuron subtypes to those identified by previous studies, we mapped
183 single-cell transcriptomes from the Coverdell et al. and Veerakumar et al. studies onto our
184 nAmb neuron clusters using reference query mapping. This method projects query cells onto
185 reference cell clusters without altering the reference data structure [45]. Interestingly, while the
186 Coverdell et al. cell clusters largely mapped to different reference cell clusters (Supplemental
187 Figure 2A) as expected, the Veerakumar et al. cells subdivided among the same three
188 reference clusters (Supplemental Figure 2B). This was surprising, since, for instance, the
189 larynx-projecting subtypes in Coverdell et al. ($Vipr2^{nAmb}$ neurons) and Veerakumar *et al.*
190 (laryngeal neurons) mapped to different reference cell clusters. When we assessed the
191 confidence of cell mapping, most Coverdell *et al.* cells mapped with high confidence (>0.8;
192 Supplemental Figure 2C) whereas most Veerakumar *et al.* cells mapped with lower confidence
193 (<0.6; Supplemental Figure 2D). This suggests that the adult nAmb neurons in Coverdell *et al*.
194 are more like the adult nAmb neurons in our present dataset than are the neonatal nAmb
195 neurons in Veerakumar *et al*., potentially due to developmental differences in gene expression.
196 In line with this possibility, the larynx-projecting neurons of Veerakumar *et al*. but not in those of
197 Coverdell et al. (Supplemental Figure 2E-F) expressed the gene *Adcyap1*, consistent with the
198 broader expression of *Adcyap1* in the developing brain [46]. Thus, the ability to match neonatal
199 and adult nAmb neurons with the reference query approach may be limited by developmental
200 differences in gene expression.
201
202 *Partially Overlapping Populations of Nucleus Ambiguus Neurons Express Npy2r and Adcyap1*
203
204 Given the likelihood that cardiovagal nAmb neurons express *Npy2r* and *Adcyap1*, we mapped
205 the transcripts of these genes in the adult mouse nAmb using RNA fluorescence *in situ*
206 hybridization (RNA FISH). First, to label peripherally-projecting neurons, including all nAmb
207 vagal efferent neurons, we intraperitoneally injected adult C57BL6/j mice with the retrograde

208 tracer Fluorogold [47,48]. We then performed RNA FISH for *Adcyap1*, *Npy2r*, and *Chat* transcripts
209 in coronal sections and imaged them throughout the nAmb's compact, semi-compact, and loose
210 subregions. We observed *Npy2r*+ nAmb vagal efferent neurons scattered throughout these
211 subregions (representative images in Figure 2A), consistent with the known anatomical
212 distribution of cardiovagal nAmb neurons [13,30,37,49]. Quantifying nAmb neurons expressing
213 *Adcyap1* and/or *Npy2r* revealed a partially overlapping distribution. Specifically, 4% of nAmb
214 neurons expressed both *Npy2r* and *Adcyap1*, 3% expressed *Npy2r* but not *Adcyap1*, and <1%
215 expressed *Adcyap1* but not *Npy2r* (Figure 2A, B). Thus, only a small minority of nAmb vagal
216 efferent neurons express *Adcyap1* and/or *Npy2r*. Of note, the 8% of nAmb neurons expressing
217 *Adcyap1* and/or *Npy2r*, extrapolated for the total number of adult mouse nAmb neurons [50],
218 would be approximately 47 neurons per nAmb, slightly below previous estimates of
219 retrogradely-labeled cardiovagal nAmb neurons in mice (50-60 neurons) [37].
220
221 *Retrograde Labeling from the Heart Reveals Cardiovagal Populations in the nAmb and*
222 *Intermediate Zone*
223
224 To identify heart-projecting vagal motor neurons, we injected the retrograde tracer Fluorogold
225 into the pericardiac fat pad near the posterior right atrioventricular junction, where cardiovagal
226 nerve endings terminate [51] (Figure 3A). One week later, we collected brainstem tissue for
227 Fluorogold immunofluorescence and RNA FISH. On average, we identified 40 ± 24 Fluorogold-
228 labeled neurons per mouse bilaterally in the nAmb, distributed across the full rostral–caudal
229 extent of the nAmb (Figure 3B; n = 3 mice). Among these, 27% contained *Npy2r* transcripts by
230 RNA FISH (Figure 3C). These results indicate that *Npy2r*+ nAmb ($Npy2r^{nAmb}$) neurons are a
231 subset of cardiovagal nAmb neurons.
232

233 Another neuronal cluster identified in our single-nuclei RNA-seq analysis, cluster n02
234 (*Vip*+/*Chat*+/*Phox2b*+), was molecularly most like Npy2r^{+} nAmb neurons (cluster n03; see
235 cladogram in Figure 1B), raising the possibility that n02 neurons are also cardiovagal. To test
236 this, we retrogradely labeled heart-projecting neurons with intracardiac Fluorogold, as described
237 above, and assessed co-localization of Fluorogold with RNA FISH for Vip, a marker for cluster
238 n02 neurons, in the ventrolateral medulla. Surprisingly, *Vip* expression was absent from
239 Fluorogold-labeled nAmb neurons (Figure 3D). Instead, we observed robust *Vip* expression in
240 Fluorogold-labeled neurons of the intermediate zone between the nAmb and the DMV, where
241 85% of Fluorogold-labeled neurons also expressed *Vip* (Figure 3D-E). These findings indicate
242 that the *Vip*+ neuron cluster (n02) corresponds to cardiovagal neurons of the intermediate zone
243 rather than the nAmb, and that their inclusion in our single-nuclei RNA-seq analysis likely
244 reflects a dissection artifact. Of note, the *Vip* gene product, vasoactive intestinal peptide (VIP),
245 contributes to parasympathetic cardiac regulation by modulating heart rate, influencing
246 intracardiac ganglion excitability, and interacting with cholinergic signaling mechanisms that
247 generate cardioinhibitory output [52,53].
248
249 Together, our retrograde-tracing results demonstrate that the heart receives vagal motor input
250 from at least two molecularly and anatomically distinct neuron populations: *Npy2r*+ neurons in
251 the nAmb and *Vip*+ neurons in the intermediate zone.
252
253 *Npy2r^{nAmb} Neurons Innervate Cardiac Ganglia*
254
255 Since retrograde tracers injected into the heart can spread to other visceral tissues and label
256 non-cardiovagal neurons [54], we performed cell-type specific anterograde tracing to confirm that
257 Npy2r^{nAmb} neurons innervate the heart. Specifically, we labeled the axons of nAmb neurons with
258 an adeno-associated virus (AAV) that Cre-dependently expresses the red fluorescent protein,

259 tdTomato (AAV9-DIO-tdTomato). We confirmed the Cre dependency of AAV9-DIO-tdTomato by
260 injecting it into the ventrolateral medulla of adult C57BL6/j mice, where we failed to observe
261 tdTomato immunofluorescence three weeks later at the injection sites (n=3 mice; Supplemental
262 Figure 3A). Next, to target this AAV to Npy2r^{nAmb} neurons, we obtained Npy2r-Cre mice [44]. We
263 validated the specificity and sensitivity of Cre expression in these mice by co-localizing *Npy2r*
264 and *Cre* transcripts by RNA FISH in the nAmb. In Npy2r-Cre mice, 92% (145 of 157) *Npy2r*
265 mRNA+ neurons were also *Cre* mRNA+, and 100% (145 of 145) of *Cre* mRNA+ cells were also
266 *Npy2r* mRNA+ (n=3 mice; Supplemental Figure 3B). These results validate the specificity of
267 AAV9-DIO-tdTomato and Npy2r-Cre mice for genetically targeting Npy2r^{nAmb} neurons.
268
269 To fluorescently label Npy2r^{nAmb} axons for anterograde tracing, we injected the ventrolateral
270 medulla of Npy2r-Cre mice with AAV9-DIO-tdTomato (Figure 4A). As a positive control, we also
271 injected the ventrolateral medulla of Chat-Cre mice [38], which express Cre activity in all nAmb
272 vagal efferent neurons [36] (Chat^{nAmb} neurons). After waiting at least three weeks for AAV
273 transgene expression, we observed tdTomato immunofluorescence in a subset of nAmb
274 neurons, identified based on their immunofluorescence of the cholinergic marker ChAT (choline
275 acetyltransferase). While some neurons outside the nAmb in Npy2r-Cre mice were also
276 tdTomato+, none were ChAT+ (Figure 4B), indicating that they were not vagal efferents and so
277 would not confound our anterograde tracing results. Importantly, we observed no tdTomato+
278 neurons in the dorsal motor nucleus of the vagus (DMV), another source of heart innervation
279 (Supplemental Figure 3C) [13,55].
280
281 To determine whether Npy2r^{nAmb} neurons innervate the heart, we then imaged
282 immunofluorescence of tdTomato and the neuronal marker protein PGP9.5 in cardiac tissue
283 from the same mice. PGP9.5 is expressed generally by neurons, including all cardiac ganglia
284 neurons in rodents [56]. We observed fibers immunofluorescent for both tdTomato and PGP9.5

285 innervating PGP9.5+ cardiac ganglia in all Npy2r-Cre mice as well as positive-control Chat-Cre
286 mice (Figure 4C; n=3 mice per genotype; at least two innervated ganglia per mouse). These
287 results indicate that Npy2r^{nAmb} neurons innervate cardiac ganglia, confirming their identity as
288 cardiovagal neurons.
289
290 *Npy2r^{nAmb} Neurons Do Not Innervate the Upper Airways or Esophagus*
291
292 Since the nAmb also contains motor neurons for the esophagus and upper airways [33-35,57,58], we
293 investigated whether Npy2r^{nAmb} neurons project to those tissues using a chromogenic
294 anterograde tracing approach. First, we injected an AAV encoding Cre-dependent placental
295 alkaline phosphatase (AAV9-FLEX-PLAP) into the ventrolateral medulla of Npy2r-Cre mice (n=3
296 mice). As a positive control, we performed the same injections in Chat-Cre mice (n=3 mice;
297 Figure 5A) [36,59]. At least 3 weeks later, we collected the medulla and en bloc tissue samples of
298 the esophagus and upper airways for histology. We observed PLAP immunofluorescence in
299 ChAT-positive neurons along the rostrocaudal extent of the nAmb (Figure 5B), but none in the
300 DMV (Supplemental Figure 4), indicating that our injections were restricted to cholinergic nAmb
301 neurons.
302
303 To visualize the axons of PLAP+ neurons, we chromogenically stained them while optically
304 clearing the esophagus and upper airways as previously described [36,60]. Consistent with
305 previous studies, we observed PLAP-stained axons from Chat^{nAmb} neurons throughout the
306 larynx, pharynx, and esophagus (n=3 mice; representative image in Figure 5C) [36]. However, we
307 did not observe any such projections from Npy2r^{nAmb} neurons (n=3 mice; representative image
308 in Figure 5D). Our anterograde tracing studies together indicate that Npy2r^{nAmb} neurons
309 innervate the heart but not the upper airways or esophagus.
310

311 *Chemogenetically Activating Npy2r^{nAmb} Neurons Lowers Heart Rate*

312

313 Since Npy2r^{nAmb} neurons innervate the heart, we investigated whether they could control heart
314 rate. To selectively target these neurons, we relied on an intersectional chemogenetics
315 approach, using an AAV which Cre- and Flp-dependently expresses the excitatory
316 chemogenetic receptor hM3Dq [51]. We first validated the specificity of this AAV by injecting it into
317 the ventrolateral medulla of Chat-Cre;Phox2b-Flp mice, targeting nAmb neurons in general by
318 their co-expression of *Chat* and *Phox2b* (Supplemental Figure 5A) [36]. We then quantified co-
319 localization of immunofluorescence for ChAT and hM3Dq-HA in the nAmb, which is the only
320 region where we observed hM3Dq-HA expression. Our results demonstrate that 91% of hM3Dq-
321 HA+ cells were also ChAT+ in the nAmb, while 9% of hM3Dq-HA+ nAmb cells were ChAT-
322 (n=132 cells in total from 5 mice; Supplemental Figure 5B-C). The small percentage of hM3Dq-
323 HA+/ChAT- cells most likely represents neurons with low ChAT expression, rather than Cre-
324 independent AAV transgene expression, since we failed to detect any hM3Dq-HA
325 immunofluorescence after injecting this AAV into the nAmb of Phox2b-Flp mice that lacked
326 Chat-Cre (Supplemental Figure 5D). These results validate our previous finding that this AAV
327 only expresses hM3Dq-HA in cells that bear both Cre and Flp recombinases [51].

328

329 Next, to selectively activate Npy2r+ nAmb neurons while measuring heart rate, we injected the
330 Cre- and Flp-dependent AAV-hM3Dq-HA into the ventrolateral medulla of Npy2r-Cre;Chat-
331 Flp;R26$^{ds\text{-}HTB}$ mice (Figure 6A). This resulted in expression of hM3Dq-HA expression in a subset
332 of nAmb neurons, mostly located in the external formation, where cardiovagal neurons largely
333 reside (Figure 6B) [61]. Of note, crossing Npy2r-Cre;Chat-Flp mice to the Cre/Flp reporter mouse
334 strain, R26$^{ds\text{-}HTB}$ (H2b-GFP) [62] resulted in H2b-GFP expression in the compact nAmb (Figure
335 6B), where esophageal motor neurons reside [34-36,63], which may be due to transient
336 developmental expression of Npy2r-Cre in the compact nAmb (lineage labeling). In contrast,

viral labeling of Npy2r-Cre;Chat-Flp neurons with hM3Dq-HA in adult mice mostly labeled neurons in the external nAmb, with relatively few in the compact nAmb, consistent with both their cardiovagal identity and our results described above from virally infecting Npy2r-Cre nAmb neurons in the anterograde tracing studies.

We next measured heart rate (HR) non-invasively in awake mice [51] while chemogenetically activating their Npy2r^{nAmb} neurons with a non-metabolizable ligand for hM3Dq, deschloroclozapine (DCZ) [64]. After acclimation to the ECG system, each mouse underwent a series of intraperitoneal injections while we recorded its HR (n=9 mice). Injecting the vehicle for DCZ into Npy2r-Cre;Chat-Flp;hM3Dq^{nAmb} mice did not significantly affect HR, relative to baseline ($HR_{Baseline}$, 728 ± 16 bpm; $HR_{veh,}$ 741 ± 11 bpm ; mean ± S.D.; Tukey post-hoc following one way repeated-measures ANOVA, p= 0.94). Subsequently injecting DCZ (5 mg/kg; i.p.), however, significantly lowered their HR to 524 ± 40 bpm (HR_{veh} vs. HR_{DCZ}, one-way repeated measures ANOVA, $p = 3.6 \times 10^{-4}$; Figure 6C-D). DCZ also significantly lowered HR from baseline levels ($HR_{baseline}$ vs. HR_{DCZ}, one-way repeated measures ANOVA, $p = 5.8 \times 10^{-4}$; Figure 6D). However, injecting DCZ into wildtype mice did not significantly alter their heart rate relative to either baseline or DCZ vehicle injection (2% DMSO), indicating that DCZ on its own does not affect heart rate (n=6 mice; Figure 6C, Supplemental Figure 5E). Our results thus indicate that activating Npy2r^{nAmb} neurons can robustly decrease heart rate.

The vagus nerve decreases HR through a canonical pathway in which postganglionic cardiac neurons inhibit sinoatrial node myocytes by activating muscarinic acetylcholine receptors. To determine whether Npy2r^{nAmb} neurons use this pathway to decrease HR, we administered methyl-atropine (“MA”; 1.0 mg/kg; i.p.), a peripherally restricted muscarinic receptor antagonist. Mice were administered DCZ and then either MA or its vehicle in separate trials while we recorded their heart rate (n=9 mice). Administering MA after DCZ significantly increased HR

363 (Figure 6E). In addition, HR after MA injection was significantly higher than after MA-vehicle
364 injection (Figure 6E). Thus, activating Npy2r^{nAmb} neurons decreases HR through a canonical
365 cardiovagal signaling pathway involving peripheral muscarinic receptors.
366
367 *Voluntary Underwater Diving Activates Npy2r^{nAmb} Neurons*
368
369 Voluntary underwater submersion elicits the diving reflex in mammals, including a powerful
370 vagal bradycardia [10]. Based on the bradycardic response we observed when chemogenetically
371 activating Npy2r^{nAmb} neurons, we hypothesized that these neurons would be activated by the
372 diving response. We tested this hypothesis by evaluating expression of the immediate early
373 gene and neuronal activation marker, *Fos*, in nAmb neurons following voluntary diving. To
374 achieve this, we trained mice to voluntarily dive up to 20 cm underwater to reach an escape
375 platform (Figure 7A). We first validated that this model evokes a diving response by measuring
376 ECG with radio-telemetry implants (Figure 7B). Heart rate decreased markedly upon initiation of
377 the dive and remained low while underwater before recovering to baseline, following a brief
378 overshoot after the mice resurfaced (n=10 mice; Figure 7A,B), consistent with previous
379 descriptions. We then performed a session of repeated diving for up to 30 mins to robustly
380 activate the diving response before perfusing mice for histology. Controls were handled and
381 allowed to explore the test chamber with a shallow water level but did not perform any dives
382 (Figure 7C). In mice that performed voluntary diving, we observed a 174% increase in the
383 proportion of Npy2r^{nAmb} neurons that expressed *Fos* (n=6-7 mice; dive vs. control, 44.5 ± 5.5%
384 vs. 16.3 ± 4.3% Npy2r^{nAmb} neurons expressing Fos, unpaired t-test, t=3.915, df=11, p=0.0024)
385 (Figure 7D,F,E). Cell counts for total Npy2r^{nAmb} neurons were similar between cases (42 ± 6 vs.
386 45 ± 6 cells per unilateral nAmb in a 1 in 3 series, unpaired t-test, t=0.3679, df=11, p=0.72), and
387 a similar proportion of FG cells expressed Npy2r between cases (17.6 ± 1.6 vs. 20.6 ± 3.5% of
388 all FG cells expressed *Npy2r*, unpaired t-test, t=0.7933, df=11, p=0.44). These data indicate that

389 Npy2r^{nAmb} neurons are activated during voluntary diving, consistent with these cells being
390 functionally important for the parasympathetic regulation of the heart.
391
392 **DISCUSSION**
393
394 This study identified cardiovagal nAmb neurons based on their molecular, anatomical, and
395 functional features. Transcriptomic profiling and clustering analysis of 1,245 *Chat* expressing
396 neurons in the ventrolateral medulla indicated nine molecular subtypes. RNA fluorescence *in*
397 *situ* hybridization (RNA FISH) showed that *Adcyap1*+ nAmb neurons and *Npy2r*+ nAmb
398 (Npy2r^{nAmb}) neurons are rare and partially overlapping populations of nAmb neurons.
399 Retrograde and anterograde tracing studies revealed that Npy2r^{nAmb} neurons innervate cardiac
400 ganglia but not the esophagus and airways. Activating Npy2r^{nAmb} neurons with intersectional
401 chemogenetics significantly decreased heart rate through a canonical cardiovagal signaling
402 pathway. Finally, voluntary underwater diving significantly increased the percentage of *Fos*-
403 expressing Npy2r^{nAmb} neurons, indicating that these neurons are activated during the diving
404 reflex. Overall, our study identifies Npy2r^{nAmb} neurons as molecular subtype which selectively
405 innervates cardiac ganglia, is activated during the diving reflex, and decreases heart rate upon
406 activation.
407
408 Our study provides a more comprehensive understanding of the molecular subtypes of nAmb
409 neurons than previously known. Two studies previously used single-cell RNA-seq to molecularly
410 classify subtypes of nAmb neurons. For instance, Coverdell et al. (2022), identified three
411 subtypes from 145 *Chat*-expressing nAmb neurons of adult mice [36]. Another study, Veerakumar
412 et al. (2023), classified three subtypes of nAmb neurons from 203 heart- or larynx-projecting
413 nAmb neurons of neonatal mice [37]. However, each of these previous studies contained far fewer
414 neurons than the nearly 1,200 found bilaterally in adult mouse nAmb [50] and so may have

underestimated the diversity of nAmb neurons. Our present study identified eight molecular subtypes of nAmb neurons and one molecular subtype of intermediate-zone cardiovagal neurons among 1,245 Chat-expressing cells, nearly doubling the number of previously recognized nAmb neuron subtypes. However, our results do not exclude the presence of rare nAmb neuron subtypes. Moreover, it remains unclear whether the composition of subtypes differs between the left and right hemispheres of the nAmb or varies with sex, particularly given that the right vagus predominantly controls heart rate more strongly than the left, e.g., [65].

Our present study provides a finer resolution of nAmb neuron subtypes than previously known. For instance, a previous study by our group identified three subtypes of nAmb neurons [5], which our integrated analysis now resolves as nine subtypes. One subtype identified in our previous dataset, Adcyap1^{nAmb} neurons, matches to multiple subtypes in the combined dataset. Another previously defined subtype, Vipr2^{nAmb} neurons, divides into two subtypes, n5 (Uts2^{nAmb}) and n6 (Stk32a^{nAmb}), in the present study. Since Vipr2^{nAmb} neurons innervate the pharynx and larynx, future studies could investigate whether the Uts2^{nAmb} and Stk32a^{nAmb} subtypes separately innervate these two upper airway regions. Interestingly, *Uts2* and *Uts2b* expression mark vocal control regions in birds [66] and are enriched in the n5/Uts2^{nAmb} cluster of mouse nAmb neurons in the current study, raising the possibility that this subtype innervates the larynx to control vocalization.

Performing label transfer method to our dataset with that of another previous study also sheds light on the functional identities of our nAmb neuron subtypes. Veerakumar and colleagues identified three functional subtypes of nAmb neurons: cardiopulmonary nAmb neurons (ACP), which cause bradycardia and bronchoconstriction; cardiovascular nAmb neurons (ACV), which cause bradycardia without bronchoconstriction; and larynx-projecting nAmb neurons [37]. Marker gene expression between the current study and Veerakumar *et al.* suggests that clusters

n03.s01 (Npy2r^{nAmb} neurons) and n03.s02 of the current study may correspond to ACV neurons (*Bche*+) and ACP (*Calb1*+) neurons, respectively, of the Veerakumar *et al.* study. However, differences in gene expression between the datasets, potentially related to age differences in mice between studies, limit our ability to compare nAmb neuron subtypes between the two studies. Also, while Veerakumar *et al.* did not detect a significant increase in Fos immunofluorescence in ACV neurons after nasal immersion in anesthetized mice, indicating a lack of involvement of ACV neurons in the diving reflex. In contrast, our results show that *Fos* RNA expression increases in Npy2r^{nAmb} neurons in response to voluntary underwater diving. If Npy2r^{nAmb} neurons are ACV neurons, as indicated by our gene expression analysis, then it is possible Npy2r^{nAmb} neurons are activated differently by nasal immersion in the anesthetized state than by voluntary underwater diving.

The activation of Npy2r^{nAmb} neurons during underwater diving is consistent with a well-characterized trigemino-cardiac reflex circuit. Nasal sensory input from the anterior ethmoidal nerve engages neurons in the medullary dorsal horn which then relay to the rostral ventrolateral medulla (RVLM), where cardiovagal preganglionic neurons lie within the external formation of the nucleus ambiguus [6,26,31,67,68]. Activation of trigeminal afferents evokes a polysynaptic excitatory glutamatergic pathway to CVNs of nAmb [69,70], confirming that these neurons serve as direct functional targets of trigemino-cardiac signaling. Together, anatomical tracing, physiological stimulation, and lesion studies point to a short, robust reflex circuit with both direct and indirect pathways from trigeminal sensory neurons to cardiac efferent neurons. These mechanisms provide a framework for understanding how somatosensory stimuli engage parasympathetic output and may help inform therapeutic use of the diving response.

Finally, the molecular profile of Npy2r^{+} nAmb neurons raises hypotheses about signaling pathways through which the vagus nerve controls heart rate. Our analysis identified several

467 genes enriched in this cluster that mediates vagal control of heart rate. For instance, *Prkg1,*
468 which encodes cGMP-dependent protein kinase I, acts as a key effector in nitric oxide (NO)
469 signaling and has been implicated in modulating cardiac contractility and autonomic control of
470 heart rate via NO-cGMP pathways [71]. Similarly, *Adcy8*, a calcium-sensitive adenylyl cyclase,
471 has been shown to affect heart rate and heart rate variability when overexpressed [72]. *Ank2*,
472 encoding ankyrin-B, plays a crucial role in targeting cardiac ion channels, transporters, and
473 signaling proteins to the membrane; loss-of-function mutations in *Ank2* can lead to a spectrum
474 of arrhythmias, including sinus node dysfunction, atrial fibrillation, and ventricular arrhythmias,
475 collectively known as "ankyrin-B syndrome" [73]. Additionally, *Dmd*, which encodes dystrophin, is
476 critical for cardiac integrity, as its deficiency underlies Duchenne cardiomyopathy, characterized
477 by fibrosis, arrhythmias, and heart failure [74]. Future studies using conditional knockouts could
478 investigate whether these genes control heart rate through their action in $Npy2r^{nAmb}$ neurons.
479

480 **AUTHOR CONTRIBUTIONS**

481

482 MJ, MKM, TCC, VAG, SBGA, and JNC designed the experiments. MJ, TCC, and JNC
483 generated the single-nuclei transcriptomics data and MJ analyzed it. MJ, MKM, TCC, SBGA and
484 MEC performed RNA FISH studies. MEC performed surgeries and chromogenic staining/tissue
485 clearing for the anterograde tracing studies. MJ, AD, MKM, and MEC performed
486 immunofluorescence. YBW and CRB injected the retrograde tracer into the cardiac fat pads.
487 MJ, TCC, and MKM validated the mouse lines. MJ, MKM, MEC, AD, KC, and AS performed
488 electrocardiography. VAG developed the diving reflex assay, DSS performed post-diving
489 histology for ISH, and MEC generated and analyzed diving reflex data. MJ, TCC, MKM, VAG,
490 SBGA, and JNC prepared the figures. MJ, MKM, TCC, SBGA, and JNC wrote the manuscript,
491 with input from all the authors.
492

493 **DECLARATION OF INTERESTS**

494

495 The authors declare no competing interests.

496

497 **METHODS**

498

499 *Experimental Model and Subject Details*

500

501 The single-cell RNA-seq experiments used 28 - 35 week old male and female B6;129S6-
502 *Chat*$^{tm2(cre)Lowl}$/J mice ("Chat-Cre"; (Jackson Laboratories, JAX, strain # 028861) [38], some of
503 which had been crossed to a nuclear reporter mouse line B6.Cg-*Gt(ROSA)26Sortm1(CAG-*
504 *HIST1H2BJ/mCherry,-EGFP/Rpl10a)Evdr*/J ("H2b-TRAP"; JAX strain #029789) [75]. The
505 fluorescent *in situ* hybridization experiments used C57BL/6J mice from the Jackson Laboratory
506 (JAX, strain # 000664). The following mouse lines were used for chemogenetic studies:
507 *Npy2rtm1.1(cre)Lbrl*/RcngJ ("Npy2r-Cre"; gift of Stephen Liberles, Harvard Medical School,
508 Howard Hughes Medical Institute) [44]; and Chat$^{em1(flp)Lowl}$ ("Chat-Flp"; gift of Bradford Lowell, Beth
509 Israel Deaconess Medical Center, Harvard Medical School) [36]; R26$^{ds\text{-}HTB}$ mice (gift of Martyn
510 Goulding, Salk Institute for Biological Studies). The anterograde tracing experiments used Chat-
511 Cre, Npy2r-Cre, and C57BL/6J mice. Unless otherwise specified, all experiments used adult
512 mice with approximately equal numbers of male and female mice. Mice were housed at 22-24
513 °C with a 12 hour light:12 hour dark cycle and unlimited access to standard mouse chow and
514 water.

515

516 *Fluorescently Labeling Nucleus Ambiguus Neurons*

517

518 To fluorescently label the nAmb *Chat*+ neurons for single-nuclei transcriptomics, two
519 approaches were used. One approach crossed Chat-Cre mice with the H2b-TRAP transgenic
520 mouse line, which Cre-dependently labels cells with mCherry-tagged histone 2B protein (H2b-
521 mCherry) and an eGFP-tagged ribosomal L10 protein. Preliminary transcriptomic analysis failed
522 to detect *Chat* expression in many Chat-Cre;H2b-TRAP-labeled cells (Figure 1A, far right
523 panel), consistent with developmental Chat-Cre activity in brain regions around the nAmb.
524 Therefore, a second labeling approach was used to enrich for nAmb *Chat*+ neurons: an AAV
525 which Cre-dependently expresses H2b-mCherry, AAV9-Syn1-FLEX-H2b-mCherry (Vigene
526 Biosciences, 3.94 x 10^{13} GC/mL), injected into the right ventrolateral medulla of eight male and
527 female Chat-Cre mice, four weeks prior to tissue collection (see "Virus Injections" section for
528 details on surgery).
529
530 *Single-Nuclei RNA-Sequencing*
531
532 Tissue samples of nAmb were collected after rapid decapitation of the mice to avoid stress- and
533 anesthesia-related changes in nuclear mRNA. Brains were immediately extracted, chilled in
534 slush, and sectioned coronally at 1 mm intervals through the nAmb's full rostral-caudal extent
535 (Bregma −6.5 mm to −8.0 mm). The brain sections were immersed in ice-cold RNAprotect
536 (Qiagen, catalog # 76106) to preserve RNA during microdissection and storage. After at least
537 30 min in RNAprotect, the nAmb was visualized under a fluorescence stereomicroscope (Zeiss
538 Discovery V8), dissected, and stored in RNAprotect overnight at 4 °C. On the next day, nAmb
539 tissue was homogenized and purified by density-gradient centrifugation into a single-nuclei
540 suspension as previously described [76,77]. The single-nuclei suspension was sorted by FACS
541 using 80 nm nozzle to collect H2b-mCherry+ nuclei in a 2 mL microcentrifuge tube. The sample
542 was then processed using 10X Genomics Chromium Next-GEM Single Cell 3' cDNA Kit v3.1
543 according to the manufacturer's instructions. 10X cDNA libraries were sequenced on an Illumina

544 Next-Seq 550 with high-output, 75-cycle v2.5 kits. Sequencing reads were demultiplexed by
545 bcl2fastq2 v2.20.0 (Illumina) and aligned to the mouse genome mm10-2020-A with 10X
546 Genomics Cell Ranger software pipeline 5.0.0 using the include-intron function (Supplemental
547 Figure 1C).
548
549 Gene expression matrices from the 10X Cell Ranger pipeline were input to Seurat v4.3.0 in R
550 (version 4.1.2) for data analysis. Genes detected in fewer than three cells, cells with fewer than
551 200 genes, and cells with more than 2% of reads mapping to mitochondrial genes (%mt) were
552 filtered out. Pass-filter data were then merged across batches and integrated to correct for
553 technical differences including batch effects [78]. The following steps were then performed: log-
554 normalization of the data; selection of the 2,000 highest-variance genes using Seurat's
555 FindVariableFeatures() function; batch integration using the IntegrateData() function in Seurat;
556 scaling of gene expression values; Principal Component Analysis (PCA) for linear reduction of
557 the dimensionality of data; cell clustering using Louvain algorithm, based on Euclidean distance
558 in the PCA space comprising the first 13 PCs and with a resolution of 1; and non-linear
559 dimensionality reduction by Uniform Manifold Approximation and Projection (UMAP) for
560 visualization in two dimensions [79].
561
562 To enrich our analysis with nAmb neurons, we included neuron clusters expressing *Slc18a3,*
563 *Isl1*, and *Chat* and excluded neuron clusters expressing *Slc32a1* and *Slc17a6* (Figure 1A). After
564 removing non-nAmb neurons, the remaining neurons were re-clustered, including the steps of
565 feature selection, PCA, clustering with the top 17 PCs and resolution setting of 0.25. Integration
566 of all nAmb neurons was performed again with 12 PCs at 0.25 resolution. Cluster relatedness in
567 PCA space was illustrated with dendrograms using Seurat's BuildClusterTree() function.
568 Differentially expressed genes in each cluster were identified using Seurat's FindAllMarkers()
569 function with the Wilcoxon Rank Sum test and p values Bonferroni-adjusted for multiple

570 comparisons. The results were filtered to only include positive marker genes expressed in a
571 minimum fraction of 0.25 cells with log2-fold change threshold of 0.25. Candidate marker genes
572 were then manually selected based on their expression specificity in each cluster.
573
574 *RNA Fluorescence In Situ Hybridization (FISH)*
575
576 RNA FISH experiments were performed on brain tissue from mice, some of which received an
577 intraperitoneal injection of 2% Fluorogold (Fluorochrome) to label peripherally projecting
578 neurons, including all nAmb vagal efferent neurons, a minimum of 5 days prior to euthanasia.
579 Mice were terminally anesthetized with ketamine (20 mg/kg) and xylazine (2 mg/kg) diluted in
580 sterile saline, followed by transcardial perfusion with 0.9% saline plus heparin and 4%
581 paraformaldehyde (Thomas Scientific). Brains were extracted and post-fixed in 4%
582 paraformaldehyde for 24 hr at 4 °C. Following fixation, brains were sectioned coronally at 30 -
583 35 um thickness on a vibratome (VT-1000S, Leica). The day before FISH, the sections were
584 rinsed in PBS and then mounted on precleaned Superfrost Plus microscope slides (Fisher,
585 catalog # 12-550-15) and left to dry overnight. An ImmEdge Hydrophobic Barrier Pen was used
586 to draw a barrier around the sections. The sections were then incubated in Protease IV in a
587 HybEZ II Oven for 30 min at 40°C, followed by incubation with target probes (*Chat*, *Phox2b*,
588 *Adcyap1*, *Npy2r*, *Phox2b, Cre,* and *Flp*) for 2 hr at 40 °C. Slides were then treated with AMP 1-
589 3, HRP-C1, HRP-C2, HRP-C3, and HRP Blocker for 15-30 min at 40 °C, as previously
590 described [80]. FITC, Cy3, and Cy5 (Perkin Elmer) fluorophores were used for probe visualization.
591 Fluorogold was imaged based on its native fluorescence. Images were taken using a confocal
592 microscope (Zeiss LSM 800). The three levels of the nucleus ambiguus correspond to the
593 following bregma levels: rostral or compact nAmb: -6.47 mm through -6.75 mm from bregma;
594 intermediate or semi-compact nAmb: -6.83 mm through -7.10 mm from bregma; caudal or loose
595 nAmb: -7.19 mm through -7.46 mm from bregma.

596

597 *Virus Injections*

598

599 Mice were generally anesthetized with ketamine (20 mg/kg) and xylazine (2 mg/kg), positioned
600 in a stereotaxic apparatus (Kopf), and locally anesthetized with long-lasting bupivicaine. A
601 pulled glass micropipette was used with a Nanoject III system to stereotaxically inject one of the
602 following viral vectors per mouse: AAV9-CAG-FLEX-tdTomato ("AAV9-FLEX-tdTomato"),
603 AddGene plasmid # 28306, RRID:Addgene_28306, a gift from Edward Boyden; AAV9-CAG-
604 FLEX-PLAP virus ("AAV9-FLEX-PLAP"), a gift from Steve Liberles and Sara Prescott; AAV9-
605 Syn1-DIO-H2b-mCherry ("AAV9-DIO-H2b-mCherry"), Vigene Biosciences, 3.94 x 10^{13} GC/m; or
606 AAV1/2-CreON/FlpON-hM3Dq-HA, Viral Vector Facility, University of Zurich and ETH Zurich,
607 catalog # vhW34-1. To span the rostrocaudal extent of the nAmb, multiple injections were made
608 at the following coordinates relative to the calamus scriptorus: anterior/posterior -2.1, -2.4, -2.7
609 mm, lateral/medial +/- 1.3 mm, and dorsal/ventral -5.8 mm, from lambda; and anterior/posterior -
610 0.1 mm, lateral/medial +/- 1.3 mm, and dorsal/ventral -0.1, -1.3 mm. AAV9-FLEX-tdTomato and
611 AAV9-DIO-H2b-mCherry virus was injected unilaterally into the ventrolateral medulla, 50 nL per
612 injection, 3 injections on the right side per mouse. AAV9-FLEX-PLAP and AAV1/2-
613 CreOn/FlpOn-hM3Dq-HA were injected bilaterally, 50 nL per injection, 6 injections total per
614 mouse. This injection strategy was designed to fully cover the nAmb, avoid the DMV, and
615 restrict viral infection to only nAmb neurons. The pipette was removed 5 minutes after each
616 injection, followed by wound closure with sutures or surgical wound glue (Vetbond). Meloxicam
617 SR (5 mg/kg; sustained release, SR) was injected subcutaneously for post-operative analgesia.

618

619 *Tissue Histology and Immunofluorescence*

620

621 Three to four weeks after AAV9-FLEX-tdTomato or AAV9-FLEX-PLAP virus injection, mice were
622 deeply anesthetized with ketamine (20 mg/kg) and xylazine (2 mg/kg) diluted in sterile saline,
623 then transcardially perfused with 0.9% saline plus heparin followed by 4% paraformaldehyde
624 (PFA) (Thomas Scientific; CAS#30525-89-4) or 10% Neutral Buffered Formalin solution; NBF
625 (Sigma-Aldrich HT501128-4L). Brains and hearts were harvested and shaken in the same
626 fixative overnight at room temperature. Brains were either sectioned on vibratome at 35 um or
627 cryoprotected in 30% sucrose on a shaker at 4 °C overnight and then sectioned on freezing
628 microtome at 35 um. Hearts were cryoprotected in 30% sucrose solution in 4 °C on a shaker for
629 2 days. Hearts were then cut with a 10 blade (Fine Science Tools, Catalog #10010-00) along
630 the dorsal ventral axis and were then embedded in optimal cutting temperature (OCT)
631 compound and sectioned on cryostat (Thermo Scientific CryoStar NX50) at 10 um intervals.
632 Slide-mounted cardiac sections were then kept at –80 °C for long term storage.
633
634 For heart immunofluorescence, slides were removed from –80 °C and placed flat on a tray in a
635 fume hood to dry at room temperature. A hydrophobic barrier was drawn to contain solutions on
636 the slide, and the slides were left to air dry for 10 min. The slides were then placed in the pre-
637 chilled Coplin jar containing acetone in –20 °C for 10 min. After 10 min, acetone was removed,
638 and the slides dried in the fume hood for 10 min. A 0.1% Sudan Black solution dissolved in 70%
639 ethanol was added for 20 min to reduce autofluorescence. Tissue was then washed three times
640 for 5 min with PBS. 0.1% PBST was prepared by dissolving 100 uL of Triton-X100 (Sigma Life
641 Sciences, catalog # 9036-19-5) in 100 ml 1X PBS (Fisher, catalog # 70-013-032). Chat-Cre and
642 Npy2r-Cre heart tissues were incubated in a blocking buffer for an hour on a shaker at room
643 temperature. The blocking buffer consisted of 5% donkey serum (Millipore Sigma, catalog #
644 S30-100ML) in 0.1% PBST. For anterograde tracing with AAV-tdTomato, the tissue was
645 incubated overnight at 4 °C on a shaker with primary antibodies against PGP9.5 (rabbit, Abcam,
646 catalog #EPR4118) and tdTomato (goat, Arigo Biolaboratories, catalog #ARG55724), both

647 diluted 1:500 in 5% Donkey blocking buffer. Similarly, for anterograde tracing with AAV-PLAP,
648 the tissue was incubated with anti-PLAP (rabbit, Abcam, catalog #AB133602) and anti-ChAT
649 (goat, Sigma Aldrich, catalog #AB144P), diluted 1:500 and 1:100 respectively, in 5% donkey
650 blocking buffer.
651
652 For brain immunohistochemistry, tissue was rinsed in PBS three times for 5 minutes on a
653 shaker at room temperature, followed by incubation in 5% blocking buffer (5% normal donkey
654 serum + 0.1% PBST) for 1 hour at room temperature on the shaker. Brain sections were then
655 incubated in primary antibody against ChAT (from goat; Sigma Aldrich, catalog # AB144P;
656 1:100 dilution), PLAP (from rabbit, catalog # AB133602; 1:500 dilution) and anti-HA (from
657 chicken, Catalog # ET-HA100; dilution 1:500).
658
659 After primary antibody incubation, heart and brain sections were then rinsed three times for 5
660 minutes in 0.1% PBST solution. Species-specific donkey secondary antibodies conjugated to
661 Alexa Fluor 488, 568 or 647 were obtained from Abcam or Invitrogen and heart and brain
662 sections were incubated in secondary antibodies (dilution 1:1000) for 2-4 hours on a shaker at
663 room temperature. After three 5 minutes in PBS washes, the tissue was mounted on Superfrost
664 Plus precleaned slides (Fisher; catalog # 12-550-15) followed by cover-slipping with Prolong
665 Gold antifade mounting media (Cell Signaling Technology, catalog # 9071S) and sealed with
666 nail polish.
667
668 *Retrograde Labeling of Heart-Projecting Neurons*
669
670 Mice were deeply anesthetized using isoflurane (2.5%) and placed in a supine position on a
671 heating pad. A thoracotomy was performed by making a small incision between the second and
672 third ribs of the right rib cages to expose the heart. A 40 uL volume of Fluorogold (1%;

673 Fluorochrome) was injected into the pericardiac fat pad near the posterior right of
674 atrioventricular junction where cardiovagal nerve endings terminate. A small cotton swab was
675 used to absorb any excess tracer to minimize non-specific labeling. The incision was closed
676 using suture and animals were returned to their home cage for recovery after surgery and
677 monitored for 3 days. Carprofen (10 mg/kg) and buprenorphine (0.1 mg/kg) were administered
678 immediately after surgery and one day post-surgery.
679
680 After week animals were perfused with ketamine (20 mg/kg) and xylazine (2 mg/kg) diluted in
681 sterile saline, followed by transcardial perfusion with 0.9% saline and heparin then 10% neutral
682 buffered formalin solution ("NBF", Sigma-Aldrich HT501128-4L). The brains were collected and
683 post-fixed for 24 hr at room temperature in 10% NBF. Following fixation, brains were transferred
684 to 30% sucrose solution for 48 hr at 4 °C on a shaker and sectioned coronally at 30 or 35 um
685 thickness on a microtome (SM2010R, Leica Biosystems) for immunofluorescence and RNA
686 FISH as described in the corresponding sections above.
687
688 *Placental Alkaline Phosphatase Staining*
689
690 Following 3-4 weeks after AAV9-FLEX-PLAP virus injection [59], mice were terminally
691 anesthetized with ketamine (20 mg/kg) and xylazine (2 mg/kg) diluted in sterile saline, followed
692 by transcardial perfusion with 0.9% saline plus heparin then 10% neutral buffered formalin
693 solution ("NBF"; Sigma-Aldrich HT501128-4L). The brains, esophagus, trachea, larynx, pharynx
694 and lungs were collected and post-fixed for 24 hr at 4 °C in 10% NBF. Following fixation, brains
695 were transferred to 30% sucrose solution for 48 hr at 4 °C on a shaker and sectioned coronally
696 at 30 um or 35 um thickness on a microtome (SM2010R, Leica Biosystems). A single series of
697 brain sections per mouse was used in histological studies to confirm injection site and PLAP

698 expression. All mice with little to no reporter expression in the nAmb were determined to be
699 surgical "misses" and so excluded from anatomical analyses.
700
701 En bloc tissue samples of the esophagus and upper airways were washed three times for 1
702 hour at room temperature in PBS, followed by incubation in alkaline phosphatase (AP) buffer
703 (0.1 M Tris HCl pH 9.5, 0.1 M NaCl, 50 mM MgCl2, 0.1% Tween 20, 5 mM tetramisole-HCl) for
704 two hours at 70 °C. Afterward, the samples were equilibrated to room temperature and then
705 washed twice in AP buffer. AP activity was visualized with NCT/BCIP solution (ThermoFisher
706 Scientific 34042) and stained samples were rinsed in AP buffer for 15 min, post-fixed in 10%
707 NBF for 1 hr, and washed in PBS. Samples were then dehydrated through a series of ethanol
708 washes (15% - 100%) and cleared using a 1:2 mixture of benzyl alcohol (Sigma-Aldrich 402834-
709 500ML) and benzyl benzoate (Sigma-Aldrich B6630-1L). Whole mount images were taken using
710 a brightfield stereomicroscope (Leica M205 FCA Stereomicroscope with color camera) and
711 brain sections were imaged using fluorescence microscope (Echo Revolve).
712
713 *Chemogenetic Experiments during Non-Invasive Electrocardiography*
714
715 AAV1/2-CreON/FlpON-hM3dq-HA was injected into the bilateral nAmb of Npy2r-Cre;Chat-
716 Flp;R26ds-HTB mice as described above. The mice were allowed to recover for 6 to 8 weeks
717 before further experimentation. A non-invasive electrocardiography system (ECGenie) was then
718 used to measure heart rate. All experiments were performed at the same time of day to avoid
719 circadian differences in heart rate. Mice were acclimated to the ECGenie recording towers for
720 three days prior to data collection. Deschloroclozapine (Tocris, Cat #7193) was prepared by
721 dissolving it in DMSO, then diluting with 0.9% sterile saline to obtain a 2% DMSO solution of
722 DCZ. DCZ-vehicle was prepared by dissolving 2% DMSO in 0.9% sterile saline. After the
723 acclimation period, mice were placed into the ECGenie recording towers for a 10 min baseline

724 recording of heart rate using Corvita data acquisition software (Mouse Specifics, Framingham,
725 MA, version 2.09). Afterwards, DCZ-vehicle was administered by intraperitoneal injection, and
726 heart rate was recorded for 20 min. DCZ was then injected (5 mg/kg; i.p.), and heart rate was
727 recorded for 60 min. Next, volume-matched injections of either vehicle (0.9% sterile saline) or
728 methyl atropine bromide (MA; 1 mg/kg, dissolved in 0.9% sterile saline) was administered, and
729 heart rate was recorded for 30 minutes. Each mouse underwent at least one trial in which MA
730 was injected after DCZ and at least one trial in which MA-vehicle was injected after DCZ. Data
731 was analyzed using EzCG Analysis Software (Mouse Specifics, Framingham, MA, version 17).
732 For all heart rate recordings, 3 - 5 seconds of ECG data was collected every three minutes.
733 ECG signals were then visually inspected for missed or ectopic beat detection. Pieces of data
734 with noisy signal or incorrect beat detection were removed before calculating heart rate, and if
735 needed, the signal was inverted.
736
737 Heart rate values were averaged per animal for each condition. Comparisons between baseline,
738 vehicle, and DCZ conditions were performed using one-way repeated-measures ANOVA,
739 followed by Tukey's honestly significant difference test for post-hoc pairwise comparisons using
740 the emmeans package in R (version 4.1.2), which computes exact Tukey-adjusted p-values. For
741 the comparisons of methyl-atropine (MA) versus MA-vehicle conditions, paired t-tests were
742 performed. A p-value < 0.05 was considered statistically significant.
743
744 To validate expression of hM3Dq, mice were euthanized, transcardially perfused, and fixed as
745 described above after completion of the ECG studies. Brains were fixed overnight, transferred to
746 30% sucrose solution for 48 hr at 4°C on a shaker, and sectioned coronally at 30 or 35 um
747 thickness on a microtome (SM2010R, Leica Biosystems). Sections were rinsed 3 times for 5
748 minutes in PBS, then incubated in blocking buffer (5% normal donkey serum + 0.1% PBST) for
749 1 hour on a shaker at room temperature. After blocking, sections were incubated overnight at 4

750 °C on a shaker in primary antibody solution containing goat anti-Chat (Primary antibody at 1:100
751 dilution in blocking buffer, Sigma Aldrich catalog # AB144P, lot # 3491643) and chicken anti-HA
752 antibody (1:500 dilution, Aves Lab, lot # HA7757994, catalog # ET-HA 100). The following day,
753 sections were rinsed 3 times for 5 minutes in 0.1 % PBST solution (100 uL Triton-X dissolved in
754 100 mL sterile PBS) on a shaker, then incubated in secondary antibody for 2-4 hours at room
755 temperature. Donkey anti-chicken Alexa Fluor 647 (Jackson ImmunoResearch, reference #
756 703-585-155, lot # 147524; 1:1000 in 0.1% PBST) and donkey anti-goat, Fluorophore 488
757 (Invitrogen, Ref# A11055, Lot#2747580; 1:1000 in 0.1% PBST). Sections were then rinsed in
758 PBS 3 times for 5 minutes on a shaker at room temperature. After rinsing, sections were
759 mounted onto slides, allowed to dry, and cover-slipped using Vectashield Antifade Mounting
760 Medium with DAPI (Cat# H-1200-10), then sealed with nail polish. Slides were imaged using the
761 confocal microscope. Mice were excluded from functional analysis if their nAmb lacked hM3Dq-
762 HA immunofluorescence, or their DMV contained more than 5 hM3Dq-HA immunofluorescent
763 neurons.
764
765 *Voluntary Dive Training*
766
767 Npy2r-Cre;Chat-Flp;dsHTB and C57Bl/6J mice were trained to voluntarily dive underwater
768 according to a protocol adapted from a previous publication [81]. A diving pool was built from a 69
769 cm long x 38 cm wide x 10 cm high plastic tub. A channel was created in the center of the pool
770 by affixing two 69 cm long x 0.32 cm wide x 10 cm high plexiglass strips with 2.5 cm
771 perpendicular ledges 6 cm from the bottom, one third and two thirds of the way across the
772 length of the pool. These served as rails along which water-level barriers were placed to extend
773 the length of the underwater dive. Squares of 10 cm x 0.6 cm x 10 cm plexiglass were used to
774 construct walls around the starting end of the pool. To set up the diving enclosure for training,
775 the two plexiglass strips were taped in place onto either end of the container and water was

added to the tank to the desired level. Water temperatures were kept between 33 °C and 37 °C to prevent hypothermia and minimize stress. A raised platform was placed at the opposite end for the mouse to climb out of the water (escape platform). Small circles were drawn every 15 cm on the inside walls of the two plexiglass strips to help guide the mice while underwater. Additionally, a large “X” was drawn on the underwater portion of the platform for the same purpose. The diving enclosure was set up with the platform and thermometer and filled with water before every dive training session; and drained and cleaned after every session. A heat lamp was set up approximately 30 cm above the recovery cages to provide warmth after dive completion. At the start of each swim or dive, the mouse was taken from its home cage, placed at the starting end of the pool, allowed to swim across to the escape platform, and then removed from the pool and placed into its home cage under the warming lamp.

A 5-day progressive protocol for dive training mice was performed as follows. On Day 1 of dive training, mice were allowed 2 min to explore the pool with 1 cm of water. If a mouse touched the escape platform with all 4 paws within 2 min, they were immediately removed from the pool. If they failed to reach the escape platform, they were removed after 2 min. This was repeated 7 times. On Day 2 of dive training, mice were allowed to explore with the same criteria as in Day 1, for two trials. Then, water was added up to 3 cm and mice were allowed to wade through the water, for two trials. Water was added up to 5 cm, so the mice were unable to touch the bottom of the enclosure while swimming, for 7 trials. On Day 3, mice underwent a series of underwater dive trials of increasing distances: one trial of a 1 cm long dive; two trials of a 3 cm long dive; four trials of a 5 cm long dive; and six trials of a 6 cm long dive. On Day 4, mice underwent one trial each of 1 cm, 3 cm and 5 cm long dives, two trials of a 1cm long dive, and 5 trials of a 10 cm long dive. On Day 5, mice did one trial each of 1 cm, 3 cm and 5 cm long dives, two trials each of a 1 cm and a 10 cm long dive, and five trials of a 20 cm long dive. Dive repetitions were increased or decreased depending on each mouse’s learning speed.

802

803 *Telemetric Electrocardiography*

804

805 After dive training completion, mice underwent surgical implantation of electrocardiography
806 (EKG) telemeters (Data Science International, DSI; ETA-F10) for wirelessly recording heart rate
807 at rest and during diving. Each mouse was anesthetized with isoflurane and placed in dorsal
808 recumbency on the auto-heated surgical table. The skin on the chest and upper abdomen was
809 shaved, cleaned with alcohol and iodine, and 0.1mL of Nocita (long-lasting Bupivacaine, 13.3
810 mg/mL) was injected at the midline of the sternum, with the limbs loosely taped down. A 2 cm
811 shallow, vertical inline incision was made along the sternum and, using blunt-tip hemostatic
812 forceps, a subcutaneous pocket starting at the left caudal edge of the incision was created down
813 the lateral flank. Once the pocket size was increased to ensure adequate fit for the probe, the
814 pocket and the probe were rinsed with sterile saline. The device ID number was noted alongside
815 the mouse ID and the probe was inserted into the pocket with the leads oriented cranially (red
816 lead on the left and white lead on the right). The leads were trimmed to the appropriate length to
817 allow for placement in desired locations. The red lead was routed subcutaneously by blunt
818 dissection to the left flank inferior to the underarm and secured with a 6.0 silk suture to the
819 muscle. The white lead was routed subcutaneously across the torso to the upper right pectoralis
820 major and secured with a 6.0 silk suture. Secure attachment of the probe was confirmed by
821 slightly tugging on the leads. The incision was closed with 3 mouse wound clips and antibiotic
822 ointment was applied. The wound clips were reapplied if dislodged by the mouse. Wound clips
823 were subsequently removed 7-10 days later.

824

825 *Diving Reflex Assay*

826

827 For diving-induced *Fos* experiments, a total of 13 mice (7 females, 6 males) were trained

828 according to the above protocol. Before training, mice were administered Fluorogold
829 systemically (FG; i.p. as described above) to label nAmb neurons. After 5-7 days of training,
830 mice were randomly assigned into groups (voluntary dive or no dive). For voluntary diving, 7
831 mice (4 females, 3 males) were introduced into the diving chamber filled with water and allowed
832 to dive voluntarily to reach the platform. Upon reaching the platform, mice were given 10-15 sec
833 rest before being returned to the opposite end of the apparatus to dive again. For 20-30 min
834 mice completed 20-40 individual dives before being placed in a warmed recovery chamber for
835 20 min to allow time for *Fos* mRNA expression. As a control ('no dive'), mice were placed in the
836 diving enclosure filled with 1 cm of water and allowed to explore for 30 min before being placed
837 in a warmed recovery chamber for 20 min before perfusion.
838
839 Mice were deeply anesthetized with a mixture of ketamine (100 mg/kg) and dexmedetomidine
840 (0.2 mg/kg) given i.p. and perfused transcardially with 4% paraformaldehyde, pH 7.4 in 100 mM
841 phosphate buffers. Brains were removed and post-fixed in the same fixative for 12-24 hr at 4 °C.
842 Brains were sectioned (30-50 μm) on a vibratome (VT-1000S, Leica Biosystems, Deer Park, IL,
843 USA), and sections were stored in cryoprotectant (30% ethylene glycol (v/v), 20% glycerol (v/v),
844 50% 100mM phosphate buffer, pH 7.4) at −20°C. Multiplex fluorescent in situ hybridization was
845 performed using RNAscope (V1 kit, Advanced Cell Diagnostics, Newark, CA, USA). Probes for
846 *Npy2r*, *Chat*, and *Fos*, and native fluorescence was used to identify Fluorogold+ cells. Serial 1-
847 in-3 sections were washed in RNase(ribonuclease)-free phosphate buffered saline, mounted on
848 charged slides, dried overnight, and processed according to the manufacturer's instructions.
849 Immediately following the RNAscope procedure, sections were rinsed and then incubated in
850 blocking solution for 10 min followed by incubation in primary at room temperature for 60 min,
851 rinsed and incubated in secondary antibodies for 30 min, rinsed and then dried overnight before
852 cover slipping. Slides were cover slipped with Prolong Gold antifade mounting media with DAPI
853 (Thermo Fisher Scientific, catalog # P3693).

All nAmb neurons on one side of the brain between the spinal decussation and facial nucleus were counted. Only cells that contained FG fluorescence and stained for *Chat* RNA were included. Presence or absence of *Npy2r* and *Fos* RNA was determined for each FG+/*Chat*+ nAmb neuron. A cell was considered *Fos*+ if it contained >5 bright *Fos* puncta.

FIGURE

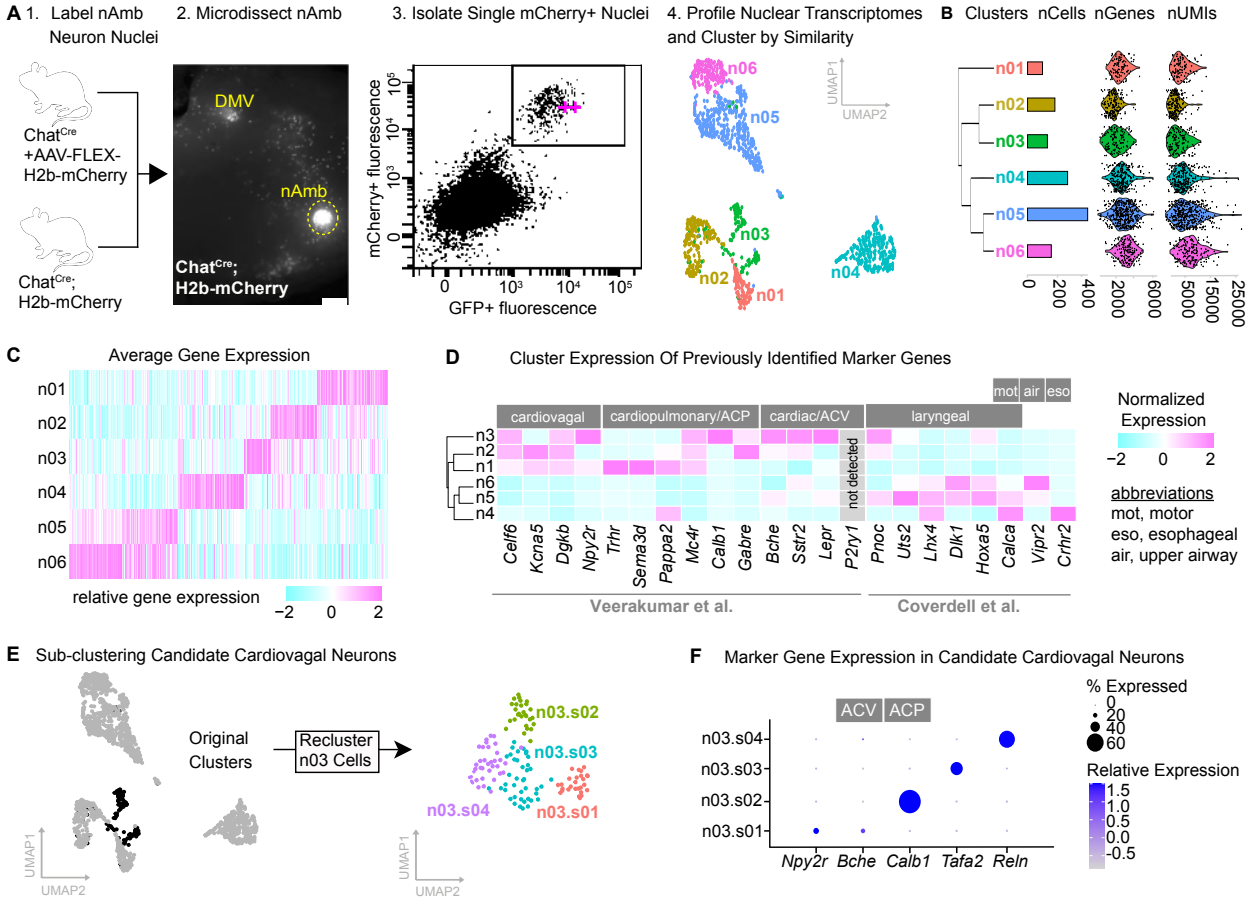

Figure 1: Molecular Classification of Nucleus Ambiguus Neurons in the Adult Mouse

A. Schematic of the single-nuclei RNA-sequencing workflow. From left to right: labeling and isolation of nucleus ambiguus (nAmb) neurons using Chat-Cre;H2b-TRAP mice and

867 Chat-Cre mice injected with a Cre-dependent AAV-H2b-mCherry; selection of
868 mCherry+/GFP+ nuclei from Chat-Cre;H2b-TRAP mice during fluorescence activated
869 nuclei sorting; uniform manifold approximation and projection (UMAP) of ventrolateral
870 medulla vagal neuron clusters.

871 B. From left to right: dendrogram illustrating relatedness of clusters; number of cells, genes
872 and unique molecular identifiers (UMIs; ~unique RNA transcripts).

873 C. All genes differentially expressed among clusters to a statistically significant extent
874 based on a Bonferroni-adjusted p-value < 0.05.

875 D. nAmb neuron cluster expression of subtype marker genes reported in previously
876 published studies.

877 E. Subclustering cells from candidate cardiovagal cluster n03.

878 F. Expression of candidate marker genes for n03 subclusters. ACP and ACV marker genes
879 labeled based on Veerakumar *et al.*

880

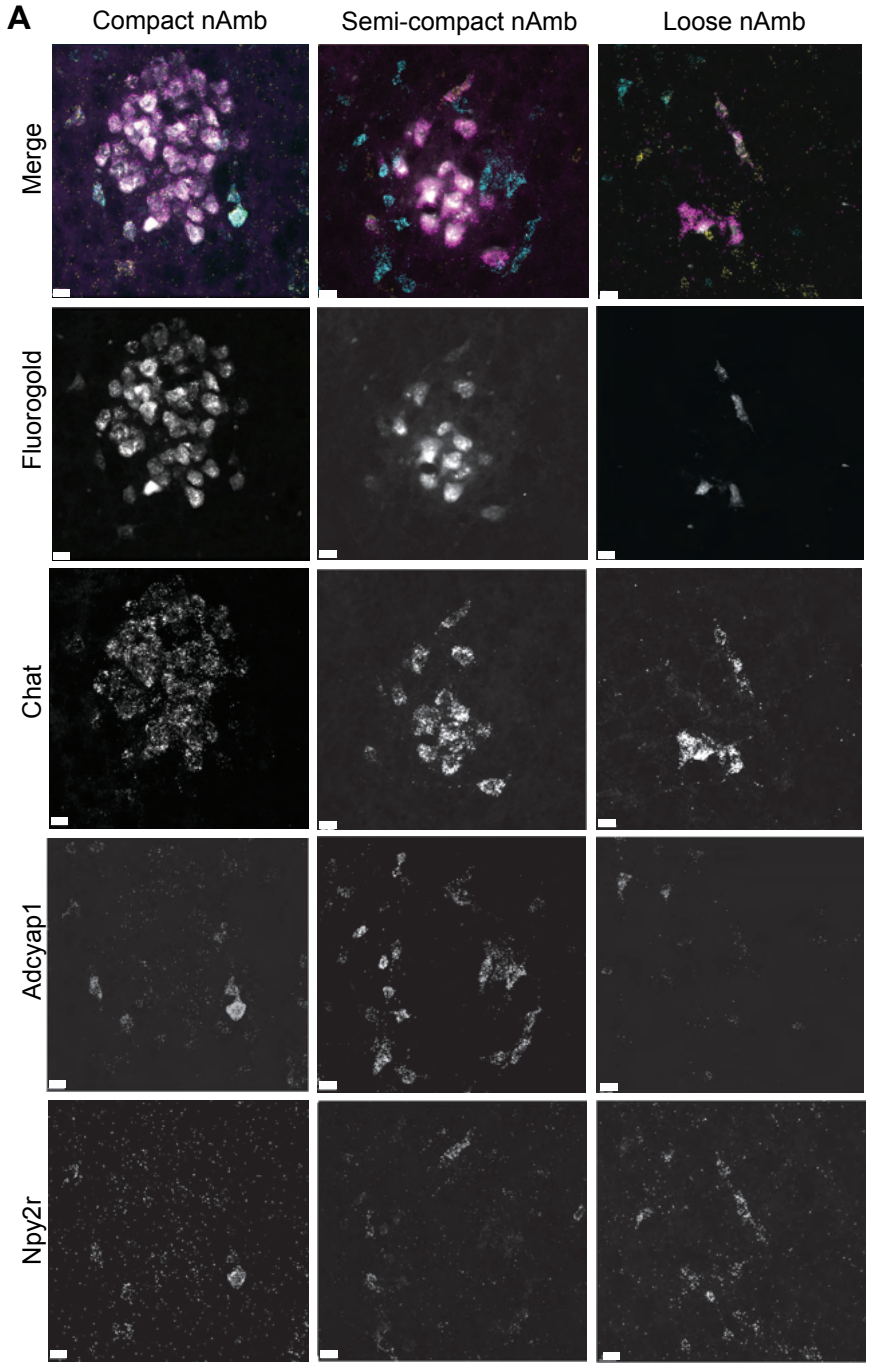
A
Compact nAmb
Semi-compact nAmb
Loose nAmb
Merge
Fluorogold
Chat
Adcyap1
Npy2r

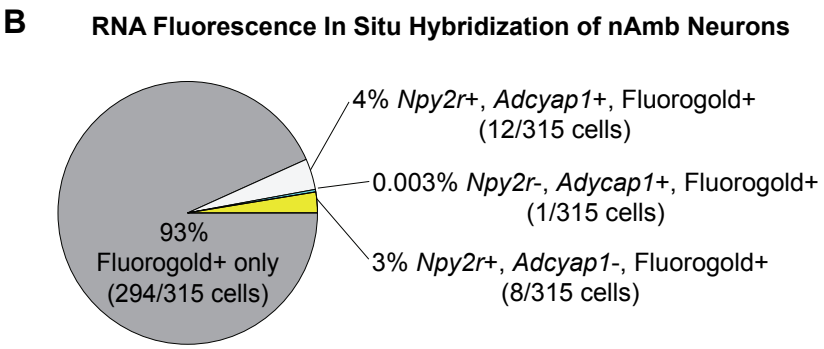
B
RNA Fluorescence In Situ Hybridization of nAmb Neurons
4% Npy2r+, Adcyap1+, Fluorogold+
(12/315 cells)
0.003% Npy2r-, Adycap1+, Fluorogold+
(1/315 cells)
3% Npy2r+, Adcyap1-, Fluorogold+
(8/315 cells)
93%
Fluorogold+ only
(294/315 cells)

881

882 **Figure 2: Partially Overlapping Populations of Nucleus Ambiguus Neurons Express**
883 ***Npy2r* and *Adcyap1***

884 A. RNAscope fluorescent in situ hybridization (RNA FISH) for *Npy2r* and *Adcyap1* in
885 compact, semi-compact, and loose subdivisions of the nAmb. All nAmb vagal efferent
886 neurons were identified by RNA FISH for *Chat* and systemic Fluorogold labeling (scale
887 bar, 20 μm). All individual color channels are displayed in grayscale. In the merged
888 image, Fluorogold is shown in grey, *Chat* in magenta, *Adcyap1* in cyan, and *Npy2r* in
889 yellow.

890 B. Quantification of RNA FISH data (n=3 mice)

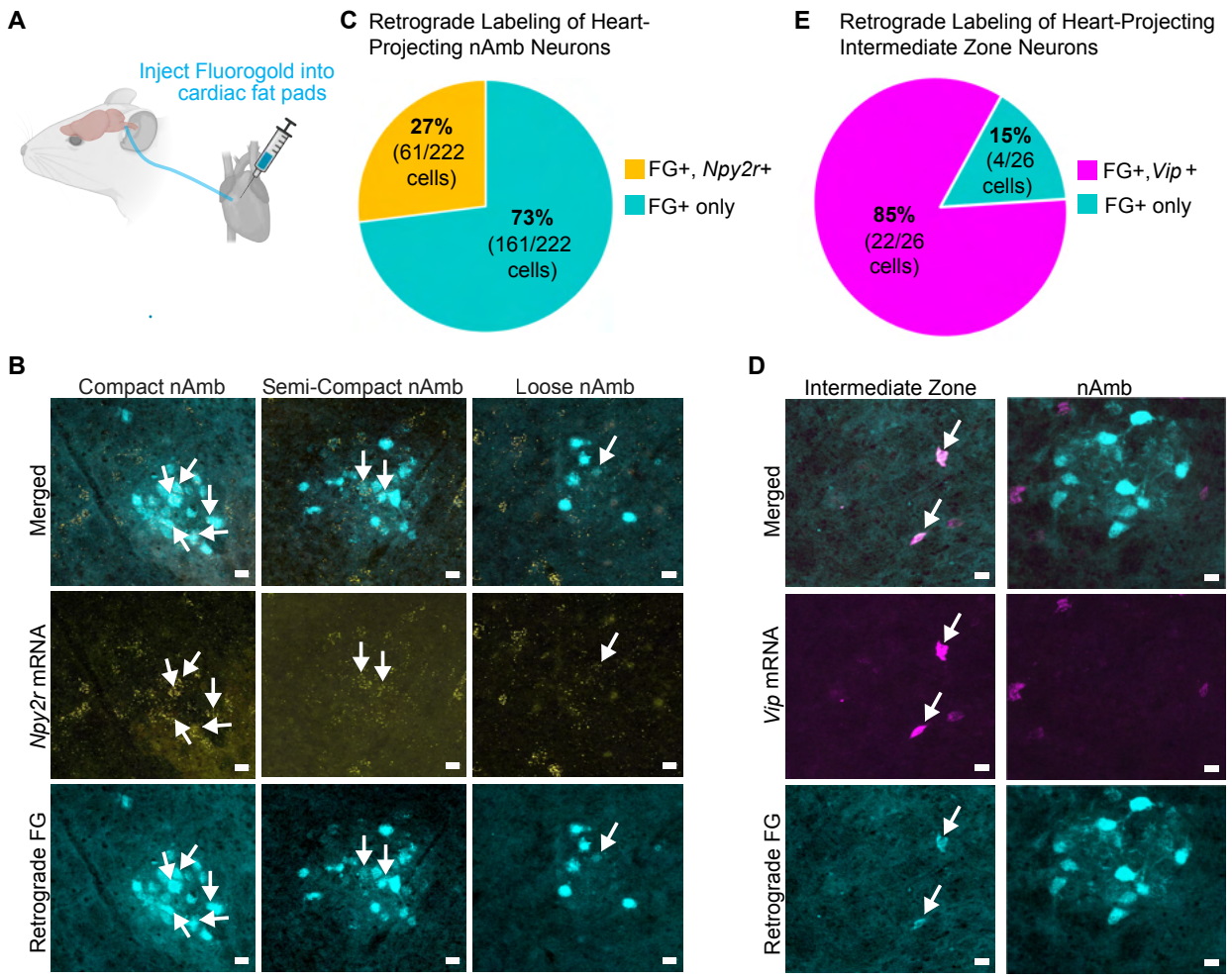

Figure 3: Retrograde Labeling from the Heart Reveals Cardiovagal Populations in the nAmb and Intermediate Zone

A. Schematic of retrograde tracing from heart with Fluorogold.

B. *Npy2r* RNA FISH and Fluorogold labeling in the compact, semi-compact and loose nAmb. Scale bar, 20 µm (n=3 mice).

C. Quantification of *Npy2r*+ cells as a subset of Fluorogold+ nAmb cells.

D. *Vip* RNA FISH and Fluorogold labeling in the compact, semi-compact and loose nAmb. Scale bar, 20 µm (n=3 mice).

E. Quantification of *Vip*+ cells labeled with retrograde Fluorogold in the intermediate zone.

A

Inject Cre-dependent
AAV-tdTomato into nAmb

Image nAmb
and cardiac ganglia

<u>Genotypes</u>
- Chat-Cre mice
- Npy2r-Cre mice

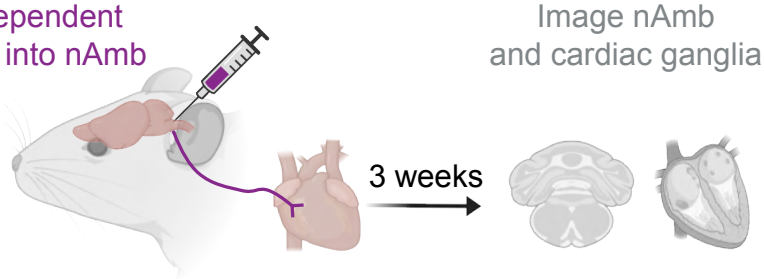

B Expression of tdTomato in cholinergic (ChAT+) nAmb neurons

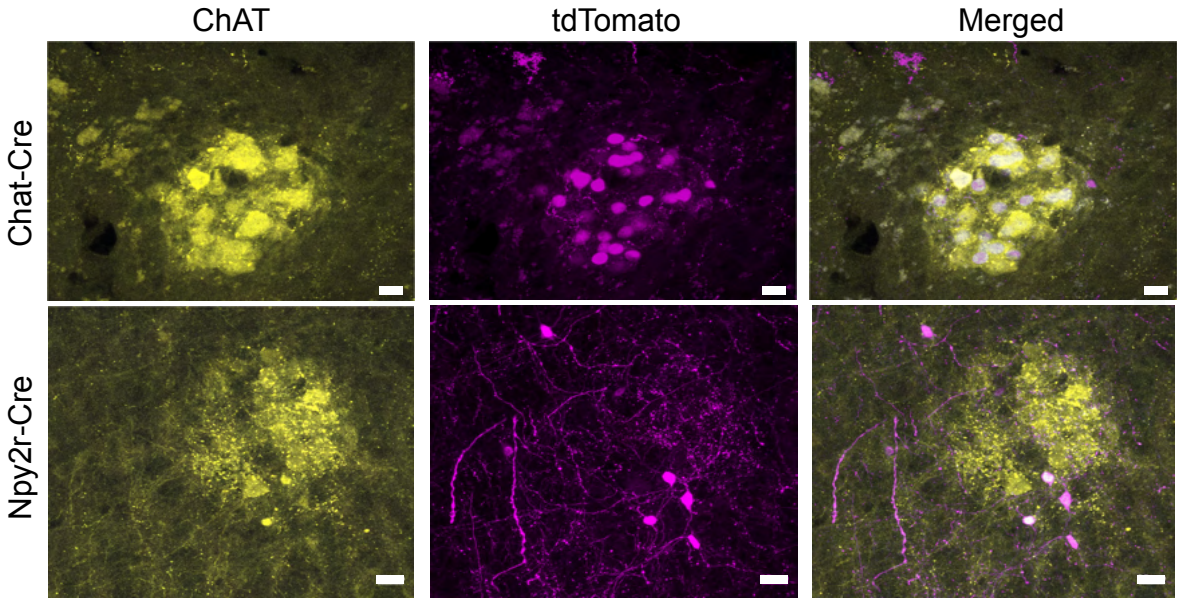

C tdTomato+ axons from nAmb neurons in cardiac ganglia

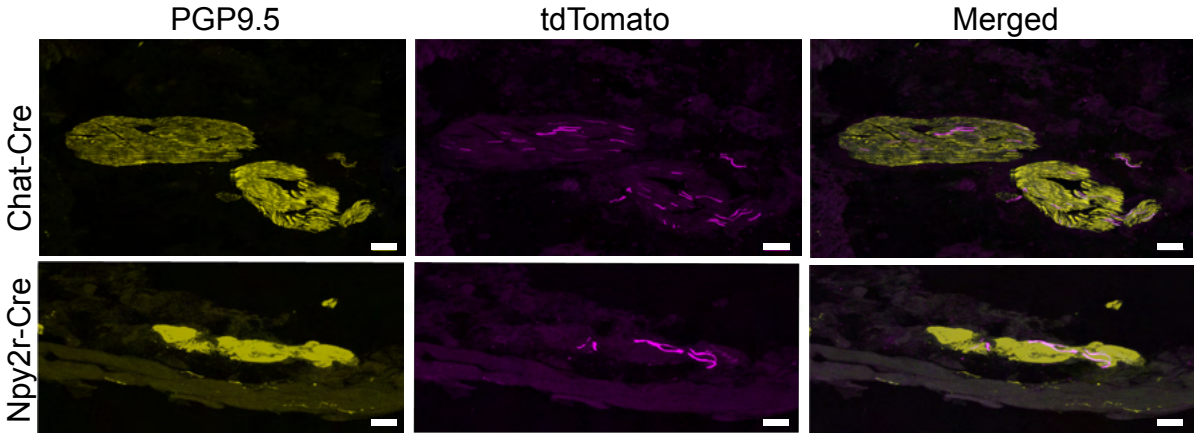

903 **Figure 4: Npy2r^{nAmb} Neurons Innervate Cardiac Ganglia**

904 A. AAV9-FLEX-tdTomato injected into right side nAmb of Npy2r-Cre mice and, as positive
905 controls, Chat-Cre mice (n=3 mice per genotype). Figure panel created with
906 Biorender.com.

907 B. tdTomato and ChAT immunofluorescence in nAmb of Chat-Cre mice and Npy2r-Cre
908 mice. Scale bar, 20 um.

909 C. tdTomato axons of Chat-Cre and Npy2r-Cre nAmb neurons in PGP9.5
910 immunofluorescent cardiac ganglia. Scale bar, 20 um.

911

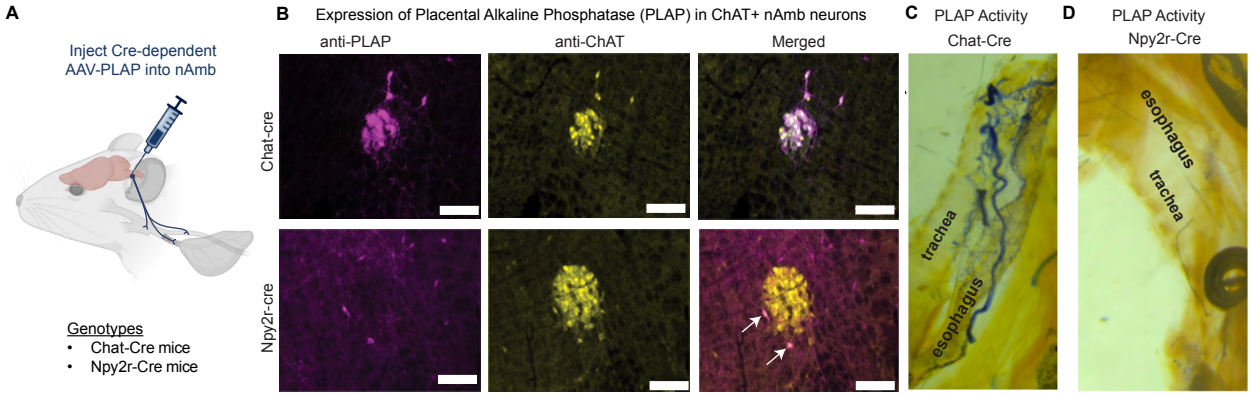

Figure 5: Npy2r^{nAmb} Neurons Do Not Innervate the Upper Airways or Esophagus

A. Strategy for targeting AAV-PLAP expression to Cre-expressing nAmb neurons of Chat-Cre and Npy2r-Cre mice. Figure panel created with Biorender.com.

B. PLAP and ChAT immunofluorescence in nAmb cells (n=3 mice). Arrows indicate double-positive cells in an Npy2r-Cre mouse nAmb. Scale bar, 70 um.

C. PLAP-stained axons from Chat^{nAmb} neurons in the upper airways and esophagus (n=3 mice).

D. PLAP-stained axons from Npy2r^{nAmb} neurons in the upper airways and esophagus (n=3 mice).

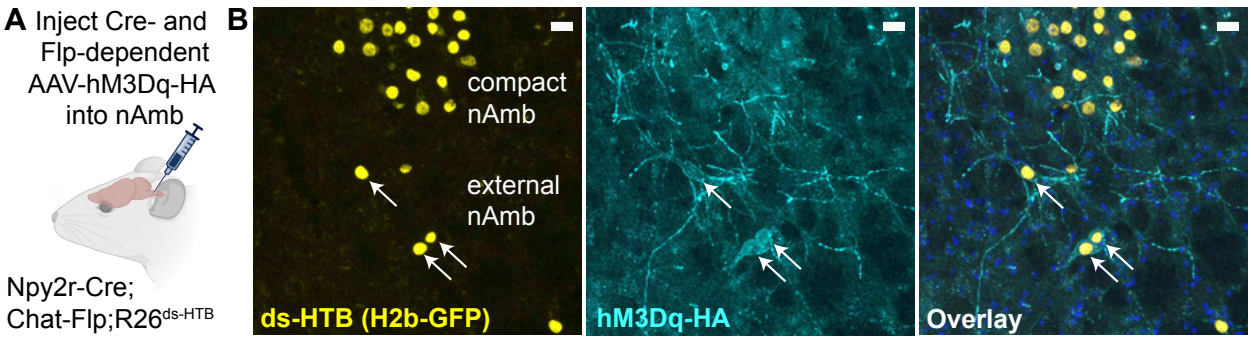
A Inject Cre- and Flp-dependent AAV-hM3Dq-HA into nAmb
Npy2r-Cre; Chat-Flp;R26ds-HTB
B
compact nAmb
external nAmb
ds-HTB (H2b-GFP)
hM3Dq-HA
Overlay

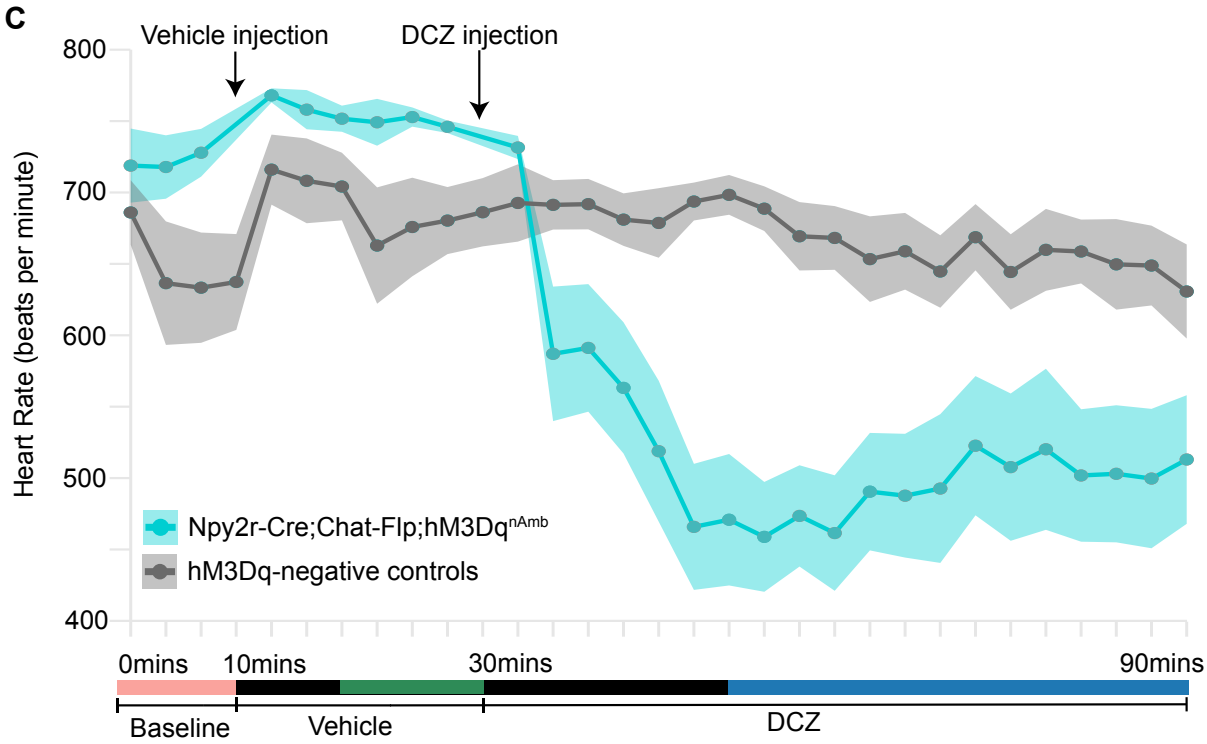
C
Vehicle injection
DCZ injection
Heart Rate (beats per minute)
800
700
600
500
400
Npy2r-Cre;Chat-Flp;hM3Dqnamb
hM3Dq-negative controls
0mins
10mins
30mins
90mins
Baseline
Vehicle
DCZ

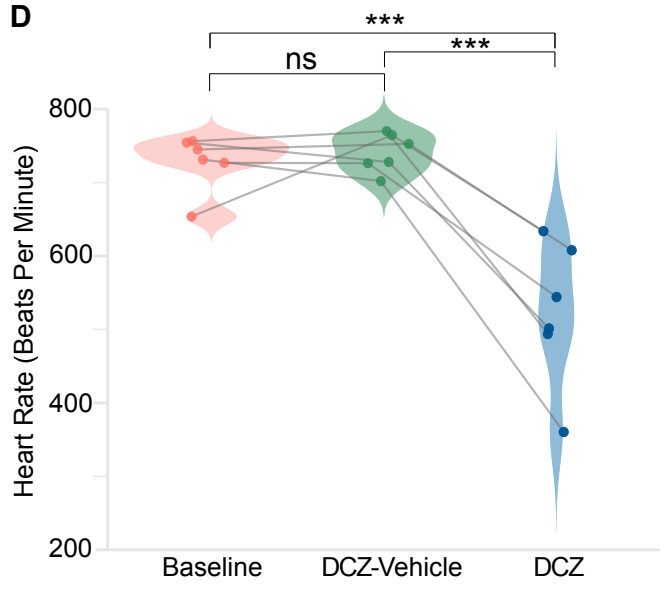
D
***
***
ns
Heart Rate (Beats Per Minute)
800
600
400
200
Baseline
DCZ-Vehicle
DCZ

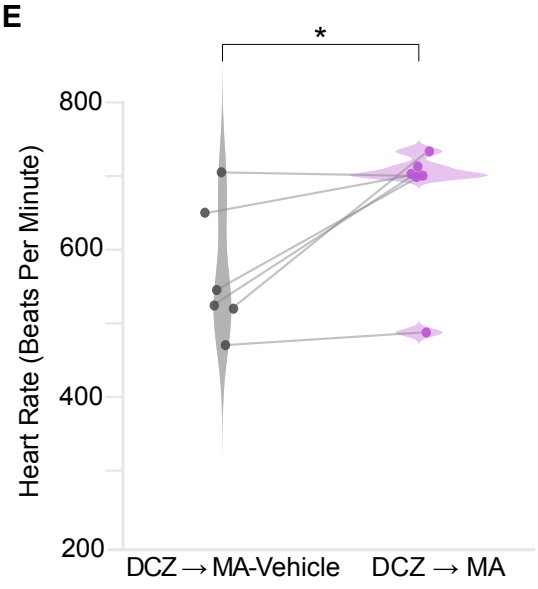
E
*
Heart Rate (Beats Per Minute)
800
600
400
200
DCZ → MA-Vehicle
DCZ → MA

923

Figure 6. Chemogenetically Activating Npy2r^{nAmb} Neurons Lowers Heart Rate

A. Schematic of experimental design. Figure panel created with Biorender.com.

B. Representative image of H2b-GFP (R26$^{ds\text{-}HTB}$ reporter) and hM3Dq-HA immunofluorescence in nAmb of Npy2r-Cre;Chat-Flp;R26$^{ds\text{-}HTB}$ mice after injecting Cre- and Flp-dependent AAV-hM3Dq-HA into their ventrolateral medulla. Arrows indicate hM3Dq-HA-positive cells. The H2b-GFP observed in the compact nAmb is likely the result of transient developmental expression of Npy2r-Cre.

C. Heart rate measured by non-invasive EKG while chemogenetically activating Npy2r^{nAmb} neurons (n=6 mice). Heart rate was recorded every 3 min, with each line representing an individual measurement across time. For statistical analyses, heart-rate values were averaged within each defined time window (baseline, vehicle, DCZ), and these window-averaged values were then used for all comparisons. The color-shaded parts of the timeline below the figure indicate the time windows used for averaging HR.

D. DCZ treatment significantly reduced heart rate relative to both baseline ($HR_{Baseline}$ = 728 ± 16 bpm; mean ± SD) and DCZ-vehicle treatment ($HR_{vehicle}$ = 741 ± 11 bpm; mean ± SD). The reduction was observed for DCZ (HR_{DCZ} = 524 ± 40 bpm; mean ± SD) with an estimated mean difference of 204.35 ± 34.9 bpm compared to baseline (one-way repeated-measures ANOVA with Tukey's post hoc test, $p = 5.8 \times 10^{-4}$, $t(10) = 5.63$) and 217.04 ± 36.3 bpm compared to vehicle (one-way repeated-measures ANOVA with Tukey's post hoc test, $p = 3.6 \times 10^{-4}$, $t(10) = 5.98$). ***, $p < 0.001$. Colors correspond to the colored parts of the timeline below panel C.

E. Administering methyl-atropine bromide (MA; 1.0 mg/kg, i.p.) rescued heart rate (HR_{MA} = 673 ± 37 bpm; mean ± SD), whereas MA-vehicle injections ($HR_{MA\text{-}veh}$ = 569 ± 36 bpm; mean ± SD) failed to reverse the bradycardia (estimated mean difference 103.64 ± 38.18 bpm, paired t-test, $t(5) = -2.71$, df= 5 $p = 0.042$). *, $p < 0.05$.

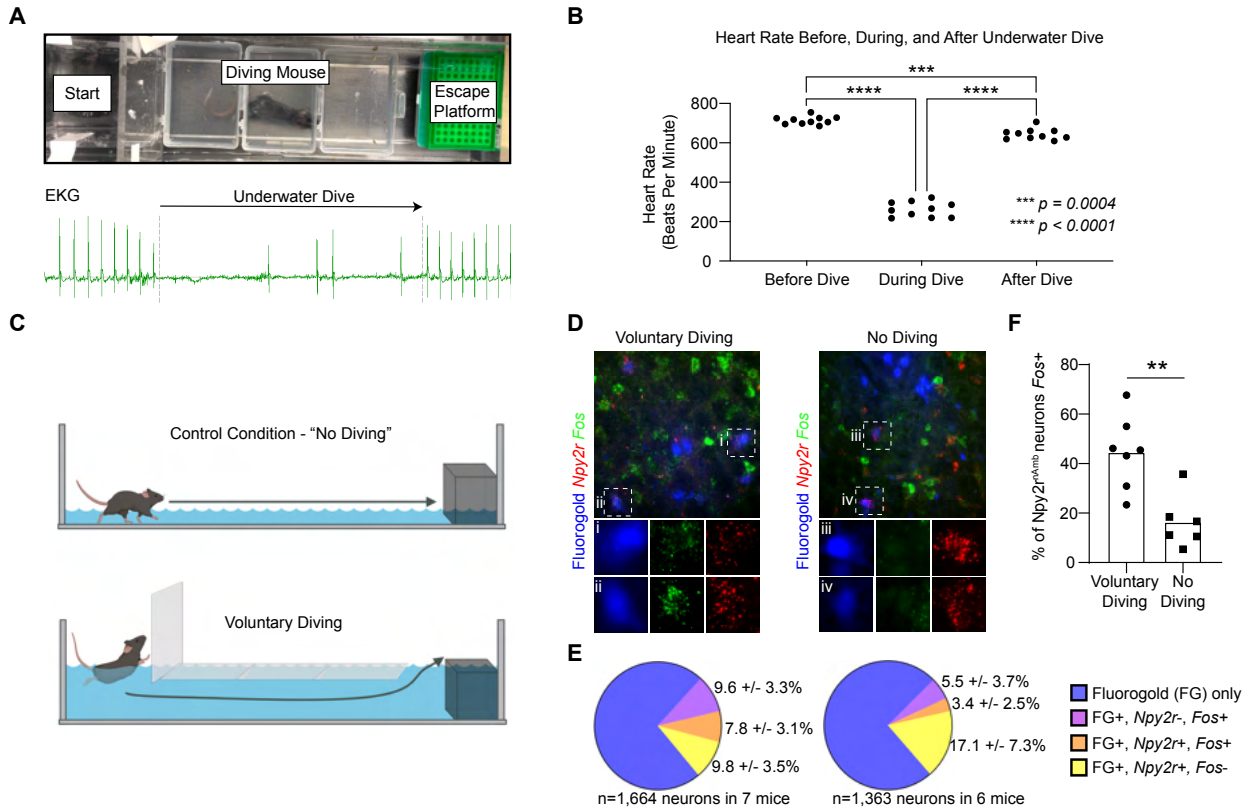

Figure 7: Voluntary Underwater Diving Activates Npy2r-Expressing Nucleus Ambiguus Neurons

A. Experimental set-up for voluntary diving assay (upper panel). EKG recorded during a voluntary dive (lower panel). EKG signal was collected using an implanted radio telemetry device.

B. Grouped data for heart rate during voluntary diving.

C. Experimental design to compare *Fos* expression in Npy2r nAmb neurons during voluntary diving and no-diving controls. Trained mice performed approximately 20-40 dives over a 20-30 min period followed by 30 min recovery period before perfusion for histology. Mice in the control condition performed no dives but were subjected to similar handling procedures. Figure panel created with Biorender.com.

D. RNA FISH of the immediate early gene *Fos* and the nAmb neuron subtype marker *Npy2r* after voluntary diving and control conditions. Systemically administered Fluorogold labels all nAmb vagal efferent neurons.

E. Quantification of *Fos* and *Npy2r* expression in Fluorogold+ nAmb neurons during voluntary diving (left) and control (right) conditions.

F. Comparison of the proportion of *Npy2r*+ nAmb neurons that expressed *Fos* in the voluntary diving and control condition. Unpaired t-test, t=3.915, df=11, p=0.002

REFERENCES

1 Weber, E. a. E. H. Experiences qui prouvent que les nerfs vague, stimulés par l'appariel de rotation galvano-magnetique, peuvent retarder et même arrêter le movement du coeur. *Arch. gen. Med.* (1846).

2 Fye, W. B. Profiles in cardiology. Ernst, Wilhelm, and Eduard Weber. *Clin Cardiol* **23**, 709-710, doi:10.1002/clc.4960230915 (2000).

3 Dampney, R. A. Central neural control of the cardiovascular system: current perspectives. *Adv Physiol Educ* **40**, 283-296, doi:10.1152/advan.00027.2016 (2016).

4 Ottaviani, M. M. & Macefield, V. G. Structure and Functions of the Vagus Nerve in Mammals. *Compr Physiol* **12**, 3989-4037, doi:10.1002/cphy.c210042 (2022).

5 Coverdell, T. C., Abbott, S. B. G. & Campbell, J. N. Molecular cell types as functional units of the efferent vagus nerve. *Semin Cell Dev Biol* **156**, 210-218, doi:10.1016/j.semcdb.2023.07.007 (2024).

6 Panneton, W. M. & Gan, Q. The Mammalian Diving Response: Inroads to Its Neural Control. *Front Neurosci* **14**, 524, doi:10.3389/fnins.2020.00524 (2020).

7 Goodwyn, E. Dissertatio medica de morteque submersorum investigandis. *Department of Medicine, University of Edinburgh, Edinburgh* (1786).

8 Vega, J. L. Edmund Goodwyn and the first description of diving bradycardia. *Journal of Applied Physiology* **123**, 275-277, doi:10.1152/japplphysiol.00221.2017 (2017).

9 Butler, P. J. & Jones, D. R. Physiology of diving of birds and mammals. *Physiol Rev* **77**, 837-899, doi:10.1152/physrev.1997.77.3.837 (1997).

10 Panneton, W. M. The mammalian diving response: an enigmatic reflex to preserve life? *Physiology (Bethesda)* **28**, 284-297, doi:10.1152/physiol.00020.2013 (2013).

11 Alboni, P., Alboni, M. & Gianfranchi, L. Diving bradycardia: a mechanism of defence against hypoxic damage. *J Cardiovasc Med (Hagerstown)* **12**, 422-427, doi:10.2459/JCM.0b013e328344bcdc (2011).

12 Geis, G. S. & Wurster, R. D. Horseradish peroxidase localization of cardiac vagal preganglionic somata. *Brain research* **182**, 19-30, doi:10.1016/0006-8993(80)90827-6 (1980).

13 Stuesse, S. L. Origins of cardiac vagal preganglionic fibers: a retrograde transport study. *Brain research* **236**, 15-25 (1982).

14 Standish, A., Enquist, L. W. & Schwaber, J. S. Innervation of the heart and its central medullary origin defined by viral tracing. *Science* **263**, 232-234, doi:10.1126/science.8284675 (1994).

15 Cheng, Z. & Powley, T. L. Nucleus ambiguus projections to cardiac ganglia of rat atria: an anterograde tracing study. *The Journal of comparative neurology* **424**, 588-606 (2000).

16 Cheng, Z., Powley, T. L., Schwaber, J. S. & Doyle, F. J., 3rd. Projections of the dorsal motor nucleus of the vagus to cardiac ganglia of rat atria: an anterograde tracing study. *The Journal of comparative neurology* **410**, 320-341 (1999).

17 Li, Y. F., LaCroix, C. & Freeling, J. Specific subtypes of nicotinic cholinergic receptors involved in sympathetic and parasympathetic cardiovascular responses. *Neurosci Lett* **462**, 20-23, doi:10.1016/j.neulet.2009.06.081 (2009).

18 Levy, M. N. Sympathetic-parasympathetic interactions in the heart. *Circ Res* **29**, 437-445 (1971).

19 Calupca, M. A., Vizzard, M. A. & Parsons, R. L. Origin of pituitary adenylate cyclase-activating polypeptide (PACAP)-immunoreactive fibers innervating guinea pig parasympathetic cardiac ganglia. *The Journal of comparative neurology* **423**, 26-39 (2000).

20 Tompkins, J. D., Ardell, J. L., Hoover, D. B. & Parsons, R. L. Neurally released pituitary adenylate cyclase-activating polypeptide enhances guinea pig intrinsic cardiac neurone excitability. *J Physiol* **582**, 87-93, doi:10.1113/jphysiol.2007.134965 (2007).

21 Feliciano, L. & Henning, R. J. Vagal nerve stimulation releases vasoactive intestinal peptide which significantly increases coronary artery blood flow. *Cardiovasc Res* **40**, 45-55, doi:10.1016/s0008-6363(98)00122-9 (1998).

22 Shanks, J., Pachen, M., Chang, J. W., George, B. & Ramchandra, R. Cardiac vagal nerve activity increases during exercise to enhance coronary blood flow. *Circulation research* **133**, 559-571 (2023).

23 Reed, C. Effects of bilateral vagotomy on blood pressure. *American Journal of Physiology-Legacy Content* **74**, 61-69 (1925).

24 Reed, C. & Layman, J. Effects of bilateral vagotomy on blood pressure and heart rate. *American Journal of Physiology-Legacy Content* **92**, 275-281 (1930).

25 Harvey, R. D. Muscarinic receptor agonists and antagonists: effects on cardiovascular function. *Handb Exp Pharmacol*, 299-316, doi:10.1007/978-3-642-23274-9_13 (2012).

26 Thomas, M. R. & Calaresu, F. R. Localization and function of medullary sites mediating vagal bradycardia in the cat. *The American journal of physiology* **226**, 1344-1349, doi:10.1152/ajplegacy.1974.226.6.1344 (1974).

27 Chen, H. I. & Chai, C. Y. Integration of the cardiovagal mechanism in the medulla oblongata of the cat. *The American journal of physiology* **231**, 454-461, doi:10.1152/ajplegacy.1976.231.2.454 (1976).

1040 28 McAllen, R. M. & Spyer, K. M. The location of cardiac vagal preganglionic motoneurones
1041 in the medulla of the cat. *J Physiol* **258**, 187-204 (1976).

1042 29 Geis, G. S. & Wurster, R. D. Cardiac responses during stimulation of the dorsal motor
1043 nucleus and nucleus ambiguus in the cat. *Circ Res* **46**, 606-611,
1044 doi:10.1161/01.res.46.5.606 (1980).

1045 30 Geis, G. S., Kozelka, J. W. & Wurster, R. D. Organization and reflex control of vagal
1046 cardiomotor neurons. *J Auton Nerv Syst* **3**, 437-450, doi:10.1016/0165-1838(81)90080-1
1047 (1981).

1048 31 Panneton, W. M., Anch, A. M., Panneton, W. M. & Gan, Q. Parasympathetic
1049 preganglionic cardiac motoneurons labeled after voluntary diving. *Frontiers in Physiology*
1050 **5**, 8 (2014).

1051 32 Lawn, A. M. The localization, in the nucleus ambiguus of the rabbit, of the cells of origin
1052 of motor nerve fibers in the glossopharyngeal nerve and various branches of the vagus
1053 nerve by means of retrograde degeneration. *The Journal of comparative neurology* **127**,
1054 293-306, doi:10.1002/cne.901270210 (1966).

1055 33 Holstege, G., Graveland, G., Bijker-Biemond, C. & Schuddeboom, I. Location of
1056 motoneurons innervating soft palate, pharynx and upper esophagus. Anatomical
1057 evidence for a possible swallowing center in the pontine reticular formation. An HRP and
1058 autoradiographical tracing study. *Brain Behav Evol* **23**, 47-62, doi:10.1159/000121488
1059 (1983).

1060 34 Fryscak, T., Zenker, W. & Kantner, D. Afferent and efferent innervation of the rat
1061 esophagus. A tracing study with horseradish peroxidase and nuclear yellow. *Anat*
1062 *Embryol (Berl)* **170**, 63-70, doi:10.1007/BF00319459 (1984).

1063 35 Bieger, D. & Hopkins, D. A. Viscerotopic representation of the upper alimentary tract in
1064 the medulla oblongata in the rat: the nucleus ambiguus. *The Journal of comparative*
1065 *neurology* **262**, 546-562, doi:10.1002/cne.902620408 (1987).

1066 36 Coverdell, T. C., Abraham-Fan, R. J., Wu, C., Abbott, S. B. G. & Campbell, J. N. Genetic
1067 encoding of an esophageal motor circuit. *Cell Rep* **39**, 110962,
1068 doi:10.1016/j.celrep.2022.110962 (2022).

1069 37 Veerakumar, A., Yung, A. R., Liu, Y. & Krasnow, M. A. Molecularly defined circuits for
1070 cardiovascular and cardiopulmonary control. *Nature* **606**, 739-746, doi:10.1038/s41586-
1071 022-04760-8 (2022).

1072 38 Rossi, J. *et al.* Melanocortin-4 receptors expressed by cholinergic neurons regulate
1073 energy balance and glucose homeostasis. *Cell metabolism* **13**, 195-204,
1074 doi:10.1016/j.cmet.2011.01.010 (2011).

1075 39 Tanaka, I., Ezure, K. & Kondo, M. Distribution of glycine transporter 2 mRNA-containing
1076 neurons in relation to glutamic acid decarboxylase mRNA-containing neurons in rat
1077 medulla. *Neurosci Res* **47**, 139-151 (2003).

1078 40 Sherman, D., Worrell, J. W., Cui, Y. & Feldman, J. L. Optogenetic perturbation of
1079 preBotzinger complex inhibitory neurons modulates respiratory pattern. *Nature*
1080 *neuroscience* **18**, 408-414, doi:10.1038/nn.3938 (2015).

1081 41 Anderson, T. M. *et al.* A novel excitatory network for the control of breathing. *Nature* **536**,
1082 76-80, doi:10.1038/nature18944 (2016).

1083 42 Herring, N., Lokale, M. N., Danson, E. J., Heaton, D. A. & Paterson, D. J. Neuropeptide
1084 Y reduces acetylcholine release and vagal bradycardia via a Y2 receptor-mediated,
1085 protein kinase C-dependent pathway. *J Mol Cell Cardiol* **44**, 477-485,
1086 doi:10.1016/j.yjmcc.2007.10.001 (2008).

1087 43 Smith-White, M. A., Herzog, H. & Potter, E. K. Role of neuropeptide Y Y(2) receptors in
1088 modulation of cardiac parasympathetic neurotransmission. *Regulatory peptides* **103**,
1089 105-111, doi:10.1016/s0167-0115(01)00368-8 (2002).

1090 44 Chang, R. B., Strochlic, D. E., Williams, E. K., Umans, B. D. & Liberles, S. D. Vagal
1091 Sensory Neuron Subtypes that Differentially Control Breathing. *Cell* **161**, 622-633,
1092 doi:10.1016/j.cell.2015.03.022 (2015).

1093 45 Hao, Y. *et al.* Integrated analysis of multimodal single-cell data. *Cell* **184**, 3573-3587
1094 e3529, doi:10.1016/j.cell.2021.04.048 (2021).

1095 46 Shuto, Y., Uchida, D., Onda, H. & Arimura, A. Ontogeny of pituitary adenylate cyclase
1096 activating polypeptide and its receptor mRNA in the mouse brain. *Regulatory peptides*
1097 **67**, 79-83, doi:10.1016/s0167-0115(96)00116-4 (1996).

1098 47 Schmued, L. C. & Fallon, J. H. Fluoro-Gold: a new fluorescent retrograde axonal tracer
1099 with numerous unique properties. *Brain research* **377**, 147-154, doi:10.1016/0006-
1100 8993(86)91199-6 (1986).

1101 48 Merchenthaler, I. Neurons with access to the general circulation in the central nervous
1102 system of the rat: a retrograde tracing study with fluoro-gold. *Neuroscience* **44**, 655-662,
1103 doi:10.1016/0306-4522(91)90085-3 (1991).

1104 49 Kalia, M. Brain stem localization of vagal preganglionic neurons. *J Auton Nerv Syst* **3**,
1105 451-481, doi:10.1016/0165-1838(81)90081-3 (1981).

1106 50 Sturrock, R. R. A comparison of age-related changes in neuron number in the dorsal
1107 motor nucleus of the vagus and the nucleus ambiguus of the mouse. *J Anat* **173**, 169-
1108 176 (1990).

1109 51 Strain, M. M. *et al.* Dorsal motor vagal neurons can elicit bradycardia and reduce
1110 anxiety-like behavior. *iScience* **27**, 109137, doi:10.1016/j.isci.2024.109137 (2024).

1111 52 Henning, R. J. & Sawmiller, D. R. Vasoactive intestinal peptide: cardiovascular effects.
1112 *Cardiovascular research* **49**, 27-37 (2001).

1113 53 Weihe, E., Reinecke, M. & Forssmann, W. Distribution of vasoactive intestinal
1114 polypeptide-like immunoreactivity in the mammalian heart: interrelation with neurotensin-

and substance P-like immunoreactive nerves. *Cell and tissue research* **236**, 527-540 (1984).

54 Grkovic, I., Fernandez, K., McAllen, R. M. & Anderson, C. R. Misidentification of cardiac vagal pre-ganglionic neurons after injections of retrograde tracer into the pericardial space in the rat. *Cell Tissue Res* **321**, 335-340, doi:10.1007/s00441-005-1145-1 (2005).

55 Nosaka, S., Yamamoto, T. & Yasunaga, K. Localization of vagal cardioinhibitory preganglionic neurons with rat brain stem. *The Journal of comparative neurology* **186**, 79-92, doi:10.1002/cne.901860106 (1979).

56 Richardson, R. J., Grkovic, I. & Anderson, C. R. Immunohistochemical analysis of intracardiac ganglia of the rat heart. *Cell Tissue Res* **314**, 337-350, doi:10.1007/s00441-003-0805-2 (2003).

57 Haxhiu, M. A., Jansen, A. S., Cherniack, N. S. & Loewy, A. D. CNS innervation of airway-related parasympathetic preganglionic neurons: a transneuronal labeling study using pseudorabies virus. *Brain research* **618**, 115-134 (1993).

58 McGovern, A. E. & Mazzone, S. B. Characterization of the vagal motor neurons projecting to the Guinea pig airways and esophagus. *Front Neurol* **1**, 153, doi:10.3389/fneur.2010.00153 (2010).

59 Prescott, S. L., Umans, B. D., Williams, E. K., Brust, R. D. & Liberles, S. D. An airway protection program revealed by sweeping genetic control of vagal afferents. *Cell* **181**, 574-589. e514 (2020).

60 Prescott, S. L., Umans, B. D., Williams, E. K., Brust, R. D. & Liberles, S. D. An Airway Protection Program Revealed by Sweeping Genetic Control of Vagal Afferents. *Cell* **181**, 574-589 e514, doi:10.1016/j.cell.2020.03.004 (2020).

61 Izzo, P. N., Deuchars, J. & Spyer, K. M. Localization of cardiac vagal preganglionic motoneurones in the rat: immunocytochemical evidence of synaptic inputs containing 5-hydroxytryptamine. *The Journal of comparative neurology* **327**, 572-583, doi:10.1002/cne.903270408 (1993).

62 Bourane, S. *et al.* Identification of a spinal circuit for light touch and fine motor control. *Cell* **160**, 503-515, doi:10.1016/j.cell.2015.01.011 (2015).

63 Lee, B. H., Lynn, R. B., Lee, H. S., Miselis, R. R. & Altschuler, S. M. Calcitonin gene-related peptide in nucleus ambiguus motoneurons in rat: viscerotopic organization. *The Journal of comparative neurology* **320**, 531-543, doi:10.1002/cne.903200410 (1992).

64 Nagai, Y. *et al.* Deschloroclozapine, a potent and selective chemogenetic actuator enables rapid neuronal and behavioral modulations in mice and monkeys. *Nature neuroscience* **23**, 1157-1167, doi:10.1038/s41593-020-0661-3 (2020).

65 Muppidi, S., Gupta, P. K. & Vernino, S. Reversible right vagal neuropathy. *Neurology* **77**, 1577-1579, doi:10.1212/WNL.0b013e318233b3a2 (2011).

1152 66 Bell, Z. W. *et al.* Urotensin-related gene transcripts mark developmental emergence of
1153 the male forebrain vocal control system in songbirds. *Sci Rep* **9**, 816,
1154 doi:10.1038/s41598-018-37057-w (2019).

1155 67 Ciriello, J. & Calaresu, F. R. Medullary origin of vagal preganglionic axons to the heart of
1156 the cat. *J Auton Nerv Syst* **5**, 9-22, doi:10.1016/0165-1838(82)90086-8 (1982).

1157 68 Panneton, W. M. *et al.* Activation of brainstem neurons by underwater diving in the rat.
1158 *Front Physiol* **3**, 111, doi:10.3389/fphys.2012.00111 (2012).

1159 69 Gorini, C., Jameson, H. S. & Mendelowitz, D. Serotonergic modulation of the
1160 trigeminocardiac reflex neurotransmission to cardiac vagal neurons in the nucleus
1161 ambiguus. *J Neurophysiol* **102**, 1443-1450, doi:10.1152/jn.00287.2009 (2009).

1162 70 Gorini, C., Philbin, K., Bateman, R. & Mendelowitz, D. Endogenous inhibition of the
1163 trigeminally evoked neurotransmission to cardiac vagal neurons by muscarinic
1164 acetylcholine receptors. *J Neurophysiol* **104**, 1841-1848, doi:10.1152/jn.00442.2010
1165 (2010).

1166 71 Layland, J., Li, J. M. & Shah, A. M. Role of cyclic GMP-dependent protein kinase in the
1167 contractile response to exogenous nitric oxide in rat cardiac myocytes. *J Physiol* **540**,
1168 457-467, doi:10.1113/jphysiol.2001.014126 (2002).

1169 72 Moen, J. M. *et al.* Overexpression of a Neuronal Type Adenylyl Cyclase (Type 8) in
1170 Sinoatrial Node Markedly Impacts Heart Rate and Rhythm. *Front Neurosci* **13**, 615,
1171 doi:10.3389/fnins.2019.00615 (2019).

1172 73 Huq, A. J. *et al.* A Novel Mechanism for Human Cardiac Ankyrin-B Syndrome due to
1173 Reciprocal Chromosomal Translocation. *Heart Lung Circ* **26**, 612-618,
1174 doi:10.1016/j.hlc.2016.09.013 (2017).

1175 74 Schultz, T. I., Raucci, F. J., Jr. & Salloum, F. N. Cardiovascular Disease in Duchenne
1176 Muscular Dystrophy: Overview and Insight Into Novel Therapeutic Targets. *JACC Basic*
1177 *Transl Sci* **7**, 608-625, doi:10.1016/j.jacbts.2021.11.004 (2022).

1178 75 Roh, H. C. *et al.* Simultaneous Transcriptional and Epigenomic Profiling from Specific
1179 Cell Types within Heterogeneous Tissues In Vivo. *Cell Rep* **18**, 1048-1061,
1180 doi:10.1016/j.celrep.2016.12.087 (2017).

1181 76 Habib, N. *et al.* Div-Seq: Single-nucleus RNA-Seq reveals dynamics of rare adult
1182 newborn neurons. *Science* **353**, 925-928, doi:10.1126/science.aad7038 (2016).

1183 77 Todd, W. D. *et al.* Suprachiasmatic VIP neurons are required for normal circadian
1184 rhythmicity and comprised of molecularly distinct subpopulations. *Nat Commun* **11**,
1185 4410, doi:10.1038/s41467-020-17197-2 (2020).

1186 78 Stuart, T. *et al.* Comprehensive Integration of Single-Cell Data. *Cell* **177**, 1888-1902
1187 e1821, doi:10.1016/j.cell.2019.05.031 (2019).

1188 79 Armstrong, G. *et al.* Uniform Manifold Approximation and Projection (UMAP) Reveals
1189 Composite Patterns and Resolves Visualization Artifacts in Microbiome Data. *mSystems*
1190 **6**, e0069121, doi:10.1128/mSystems.00691-21 (2021).

1191 80 Wang, F. *et al.* RNAscope: a novel in situ RNA analysis platform for formalin-fixed,
1192 paraffin-embedded tissues. *J Mol Diagn* **14**, 22-29, doi:10.1016/j.jmoldx.2011.08.002
1193 (2012).

1194 81 Hult, E. M., Bingaman, M. J. & Swoap, S. J. A robust diving response in the laboratory
1195 mouse. *J Comp Physiol B* **189**, 685-692, doi:10.1007/s00360-019-01237-5 (2019).

1196